Development and Assessment of a Soot Emissions Model for Aircraft Gas Turbine Engines

by

Bastien Martini

Diplomé de l'Ecole Polytechnique (2008)

Ecole Polytechnique, Palaiseau, France

Submitted to the Department of Aeronautics and Astronautics
in Partial Fulfillment of the requirements for the degree of
Master of Science in Aeronautics and Astronautics

At the
MASSACHUSETTS INSTITUTE OF TECHNOLOGY
[June 2008]
MARCH 2008

© 2008 Massachusetts Institute of Technology. All rights reserved.

The author hereby grants to MIT permission to reproduce
and to distribute publicly paper and electronic
copies of this thesis document in whole or in part.

Signature of Author.....
Department of Aeronautics and Astronautics
March 2008

Certified by.....
Ian Waitz
Jerome C. Hunsaker Professor and Department Head
Aeronautics and Astronautics
Thesis Supervisor

Accepted by.....
Prof. David L. Darmofal
Associate Department Head
Chair, Committee on Graduate Students

Development and Assessment of a Soot Emissions Model for Aircraft Gas Turbine Engines

by

Bastien Martini

Submitted to the Department of Aeronautics and Astronautics
on March 27, 2008 in Partial Fulfillment of the
Requirements for the Degree of Master of Science in
Aeronautics and Astronautics

Abstract

Assessing candidate policies designed to address the impact of aviation on the environment requires a simplified method to estimate pollutant emissions for current and future aircraft gas turbine engines under different design and operating assumptions. A method for NO_x and CO emissions was developed in a previous research effort. This thesis focuses on the addition of a soot mechanism to the existing model. The goal is to estimate soot emissions of existing gas turbine engines within soot measurement uncertainties, and then to use the method to estimate the performance of potential future engines.

Soot is non-volatile primary particulate matter. In gas turbine engines the size rarely exceeds 1μm. The soot is composed almost exclusively of black carbon, is an aggregate of nearly spherical carbon primary particles, and exhibits fractal behavior. Results of other studies regarding soot nucleation, growth, oxidation, and coagulation rates are integrated within a network of perfectly-stirred reactors and shown to capture the typical evolution of soot inside a gas turbine combustor, with soot formed in the early parts of the combustor and then oxidized.

The soot model shows promising results as its emissions estimates are within the measurement uncertainties. Nevertheless, model uncertainties are high. They are the consequence of the large sensitivity to input variables. Therefore, the validity of the model is limited to cases with available engine data. More engine data are needed to develop and assess the soot model.

Thesis Supervisor: Ian Anton Waitz

Title: Jerome C. Hunsaker Professor of Aeronautics and Astronautics and Head of the Aeronautics and Astronautics Department

Acknowledgements

There are many people that I want to thank for my research at MIT. First, I cannot express enough gratitude to Pr. Waitz who made this project possible. He trusted me and showed me encouragement and patience even when I struggled. He was always here to answer my emails and give great orientations to my research. His workload is impressive and I still do not know how he has been able to carry out all his tasks and still have time to advice me. I am sorry for the numerous times I spammed him.

I also want to thank Pr. Willcox. She is co-director of the project and always gave me great advice. I am also glad she loves Annecy (my home town in France) so much. Other professors such as Pr. Jacobson and Dr. Dobbins from Brown University participated at one point to my work and I thank them for it.

Joe Palladino was of great help during all my research at MIT. His aircraft engine knowledge is tremendous and his help was precious. I cannot thank him enough.

I also want to express my gratitude to all the people who helped me during my research and I apologize for not being able to list them all. Dr. Jim Hileman was always here to take a coffee break to talk, Julien helped me get into PARTNER, Anuja loved talking about babies, Chris S. never took more than 5 minutes to answer my emails, and I had great talks with Tim and Phil from EDS.

Then, my friends made a great time at MIT wonderful. My coworker, the best person I have ever met at MATLAB®, helped me on my research, helped me to understand a mumbling Bostonian, to show me the U.S., to make me fly, to make me love football and so many other things that it would take a thesis to list them all. Jim did it too, being always present to help my wife and I, to play football, to laugh to my bad jokes and so many other things that I forget. Melissa, Michelle, Alex, Ana, the French guys made me have a great time in Boston.

Finally, I cannot thank enough my wife Adeline and my son Clément. My wife has accepted to come to Boston and set aside her career to live with me. She was always here to cheer me up and to make me understand that there is something else than studies and sport. She also gave me the best present I ever got: my son.

Table of Contents

Abstract 3
Acknowledgements 5
Table of Contents 7
List of Tables 9
List of Figures 11
Nomenclature 15
List of Acronyms 17
Introduction 19
1.1. APMT and EDS 20
1.2. Research motivation 21
1.3. Emission Regulation 21
1.4. Smoke Number 23
1.5. Previous Work 24
1.6. Thesis Objective 26
1.7. Organization of the Thesis 27
Particulate Matter (PM) 29
2.1. Definition and Classification 29
2.2. Health and Climate Issues Related to PM 31
2.3. Measurement of Non-Volatile PM for Aircraft Engines 32
Soot Formation 35
3.1. Soot Properties 35
3.2. Soot Formation Pathway in Aircraft Combustors 37
3.2.1. Precursors 38
3.2.2. Nucleation 41
3.2.3. Growth, Oxidation, and Coagulation 42
3.3. Modeling Rates of Soot Formation inside the Combustor 44
3.3.1. Nucleation 45
3.3.2. Growth: HACA Soot Particle Surface Mechanism 48

3.3.3. Oxidation Mechanism 53
3.3.4. Coagulation Mechanism 56
3.3.5. Lindstedt's Model 56
3.3.6. Modeling Summary 57
3.4. Discussion of the Physical Parameters Impacting Soot Formation 58
Insertion of the Soot Model 61
4.1. The Combustor Model 61
4.2. Computation of Soot Emissions in PSRs and PLUGs 64
4.2.1. Soot Modeling Integral Equations 65
4.2.2. Relation between Soot Flows and Soot Densities 67
4.2.3. Soot Equations System 68
4.3. Chemical Kinetics Models 69
Results Discussion 71
5.1. Selection of the Soot Model 71
5.1.1. Selection of the Kinetics Model 71
5.1.2. Choice of the Soot Formation Model 72
5.1.3. Selection of the Unmixedness Representation 74
5.1.4. Choice of the Fuel Model and Aromatics Representation 80
5.2. Correction of the Model 82
5.3. Problems of Sensitivity to Input Variables 86
5.3.1. Sensitivity Correction and New Results 89
5.3.2. Interpretation and Precision Estimation of the Model 92
Conclusion 97
Appendixes 99

List of Tables

Table 1 – Major PM compounds found in aircraft exhaust..... 31
Table 2 – Assumed air-to-fuel ratios by power setting..... 34
Table 3 - Examples of simple PAHs..... 39
Table 4 - Representative Chemical Limits for Aircraft fuels..... 40
Table 5 - Soot reaction mechanism from Colket and Hall with a reaction rate of k = A.exp(-E/(RT))..... 49
Table 6 - Soot reaction mechanism from Kazakov et al. with a reaction rate of k = $A.T^n.exp(-E/(RT))$..... 51
Table 7 - Extrapolation of $\alpha_{FW}(T)$..... 52
Table 8 – Comparison of HACA and Lindstedt's models for mass soot rates..... 57
Table 9 – Comparison of HACA and Lindstedt's models for particle soot rates..... 57
Table 10 – PW4090 and CFM56-2 models: maximum equivalence ratios for the 4 ICAO points..... 80
Table 11 – Soot model elasticity of input variables for the PW4090 engine..... 86
Table 12 – Multiplicative coefficients applied to the mass and particle soot rates found in paragraph 3.3.6..... 90

List of Figures

Figure 1 –SFC and Smoke Number improvements for aircraft engines 19
Figure 2 – APMT Architecture Overview[4]. 21
Figure 3 - Landing and Take-Off Cycle 22
Figure 4 – Inputs and outputs of the combustor model 25
Figure 5 – Schematic of Allaire's network reactor model[7] 26
Figure 6 - TEM photographs of soot aggregates at maximum soot volume fraction location along the axis of different flames, showing the texture of soot particles 36
Figure 7 - Structure of a soot primary particle 37
Figure 8 – Sooting effects of aromatics and hydrogen fuel content (from A. Lefebvre, Gas Turbine Combustion) 40
Figure 9 – Micrographs of soot particles captured on carbon grids, from an ethene diffusion flame. The transition from precursor particles to soot aggregates occurs between Z = 30 and 40 mm 42
Figure 10 – Typical TEM photographs of soot aggregates along the axis of the ethylene-fueled laminar jet diffusion flame burning in air at atmospheric pressure[38]: 43
Figure 11 – Soot formation path 44
Figure 12 – Nucleation energy activation estimation for HACA model for laminar premixed and diffusion flames[17] 47
Figure 13 – Soot surface growth rates (corrected for soot surface oxidation) in terms of the HACA mechanism of Colket and Hall for laminar flames at atmospheric pressure (from) 50
Figure 14 – Estimation of $f(T)$[31] 53
Figure 15 – Collision efficiencies as a function of distance from the burner exit, assuming that soot surface oxidation is only due to attack by OH (from 34) 56
Figure 16 – Different areas inside the combustor 63
Figure 17 – Functional outline of the combustor model 64
Figure 18 – Volume _ 65

Figure 19 – C_2H_2 differences for the simple and the complex kinetics mechanism. Residence times are obtained for TO conditions. Molar fractions are representative of other modes as well. 72
Figure 20 - Formation of soot in PSRs for both soot models 73
Figure 21 - Fraction of flow going into PSRs for a truncated normal distribution. Note the importance of the PSRs with equivalence ratios close to the mean and the very low importance of low and high equivalence ratios 75
Figure 22 – Beta distributions for different values of α and β obtained with MATLAB® 77
Figure 23 – Formation of soot in the primary zone for TO and AP powers. Note that soot emissions for takeoff and approach are more stable for the beta distribution than for the normal distribution 79
Figure 24 – PW4090: Beta pdf used to model ICAO modes emissions. Note that the maximum equivalence ratio has been increased to 2.5 in order to more accurately represent soot emissions. 80
Figure 25 – Influence of addition of acetylene on soot EI. Y-axis is normalized by the engine maximum EI obtained without acetylene addition. 81
Figure 26 – Comparison of acetylene molar fraction as function of equivalence ratios for a propane fuel containing 10% of acetylene in volume and propane fuel containing no acetylene. Note that logarithmic scales are different for the plots 82
Figure 27 – Similarities of NOx emissions for different modes, relation between unmixedness and NOx EI 83
Figure 28 – Soot emission indices as function of unmixedness for different modes, relation between unmixedness and soot EI 84
Figure 29 – Ultra sensitivity of the model when optimizing both soot and NO_x emissions 84
Figure 30 – PW4090: Soot emissions as function of fuel flow. 85
Figure 31 – CFM56-2C: Soot emissions as function of fuel flow. Note that low power problems are also found in the NO_x model. 86
Figure 32 – Elasticity of input parameters relative to soot formation in PSRs 87

Figure 33 – Evolution of soot mass flow inside the PW4090 combustor model. Note the height of the peak. 88
Figure 34 – Evolution of soot mass flow inside the CFM56-2C combustor model. 89
Figure 35 – Evolution of soot mass flow inside the new PW4090 combustor model 90
Figure 37 – Improvement of the model sensitivity for the PW4090 engine. The maximum absolute elasticity is 12.6 for the new model, compared to 83.9 for the previous one 91
Figure 39 – PW4090: emission index evolution as function of fuel flow 91
Figure 40 – CFM56-2C: emission index evolution as function of fuel flow 92
Figure 39 – PW4090: parameters picked by the optimizer for volume and air fractions . 93
Figure 40 – CFM56-2C: parameters picked by the optimizer for volume and air fractions 93
Figure 41 - Unmixedness as function of relative thrust for both engine models 94

Nomenclature

Constants

k_B	Boltzmann Constant	= $1.38*10^{-23}$ J/K
N_A	Avogadro Number	= $6.02*10^{23}$ part/mol)
R	Gas Constant	= 8.31 J/(K*mol)
ρ_s	Density of soot particles	= 1820 kg/m^3

General Variables

A	Area
A_s	Soot Surface Area per Volume (m^{-1})
d_P	Diameter of a soot particle
f_s	Soot volume fraction
k_i	Reaction Rate Coefficient of reaction *i*
K_i	Reaction equilibrium constant
M	Soot density (kg/m^3) (M = $\rho . f_s$)
M_j	Molecular weight of species *j*
M_P	Mass of an incipient soot particle
N	Soot particle density ($part/m^3$)
ρ	Fluid density
ϕ	Fuel-to-Air equivalence ratio
_	Collision efficiency

List of Acronyms

AEDT – Aviation Environmental Design Tool
AFR – Air to Fuel Ratio
APMT – Aviation Environmental Portfolio Management Tool
CI – Concentration Index (in mg/m^3)
CO – Carbon Monoxide
EDS – Environmental Design Space
EI – Emission Index (in *g/kg of fuel*)
EPA – U.S. Environmental Protection Agency
FAA – Federal Aviation Administration
FOA – First Order Approximation model
Foo – Rated Thrust
HACA – H abstraction, C_2H_2 addition chemical mechanism
LTO – Landing Take-Off
MIT – Massachusetts Institute of Technology
NO_x – Nitrogen Oxides
PAH – Polycyclic Aromatic Hydrocarbon
PLUG – 1D Reactor
PM – Particulate Matter
PSR – Perfectly Stirred Reactor
Q – Core Exhaust Volume per Mass of Fuel
RO – Rated Output
SFC – Specific Fuel Consumption
SLS – Sea Level Static
SN – Smoke Number
SO_x – Sulfur Oxides
TIM – Time In Mode
UHC – Unburned Hydrocarbons
VOLPE – Volpe National Transportation Systems Center, Environmental Measurements and Modeling Division

Chapter 1

Introduction

Aviation transportation has achieved remarkable improvements since 1960, as it is now about 70% more fuel efficient to fly than 50 years ago as shown in Figure 1. Low pollutant emissions have been achieved thanks to technology improvement, and emissions like carbon monoxide, unburned hydrocarbons, and soot have been significantly decreased. Emissions of soot (as measured by the Smoke Number) have been lowered by as much as 85% between 1960 and 2000 as shown in Figure 1. However, growth of air traffic – estimated to be 4 to 5% annually between 1980 and 2000 – has outpaced the improvement of technology and total emissions have increased. Therefore, concerns about aviation's contribution to climate change and surface air quality have increased.[1]

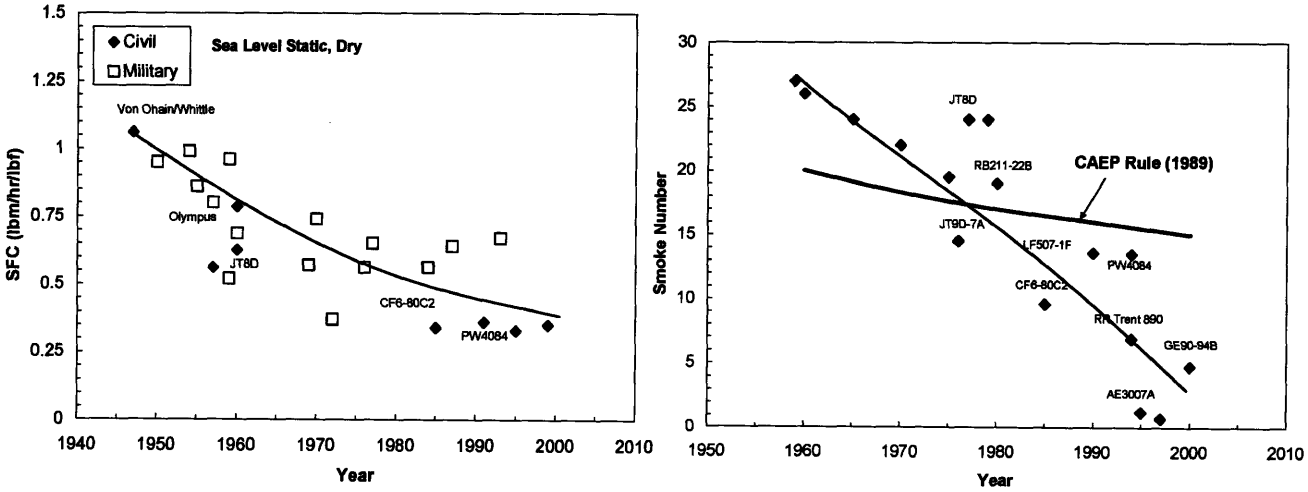


Figure 1 –SFC and Smoke Number improvements for aircraft engines[2]

[1] Aviation and the Environment: A National Vision Statement, Framework for Goals and Recommended Actions," *Report to the United States Congress*, on behalf of the U.S. DOT, FAA and NASA, by I. A. Waitz, J. Townsend, J. Cutcher-Gershenfeld, E. M. Greitzer and J. L. Kerrebrock, December 2004.
[2] from JOURNAL OF AIRCRAFT, Vol. 41, No. 1, January–February 2004, Progress in Aeroengine Technology (1939–2003), Dilip R. Ballal and Joseph Zelina

FAA, in partnership with Transport Canada and NASA, has initiated the development of a suite of tools to help assess impacts of proposed environmental policies. This thesis presents the development of a combustor model that is integrated into one component of this tool suite. The combustor model estimates emission indexes of current and future aircraft engines given one-dimensional gas turbine engine thermodynamic cycle information, combustor volume, compressor discharge pressure and temperature, fuel flow and air flow at the combustor inlet.

1.1. APMT and EDS

One of the challenges in assessing environmental policies is the long time before the outcomes of a policy can be measured directly. For aviation, this time is particularly true because the time between development and introduction of new aircraft and engine technology can be as long as 25 years. Further, after new aircraft are introduced, they may have a service lifetime of 20-30 years. Therefore, when environmental policies are introduced, the consequences can be long-lasting. This heightens the need for decision makers to carefully assess a range of policy case scenarios and to estimate the impacts of new environmental policies on aircraft technologies, operations, industry economics, and environmental impacts. For this reason, FAA, Transport Canada and NASA initiated the development of an analytical tool suite that can estimate interdependencies amongst emissions, between noise and emissions, and that can analyze the benefit-cost of proposed actions. The Aviation Environmental Portfolio Management Tool (APMT) is a component of this tool suite and provides a "thorough appraisal of all aviation-related environmental effects and their direct economic costs to the aviation industry and consumers.[3]" Among the tools that APMT uses is Environmental Design Space (EDS), which provides "estimates for source noise, exhaust emissions, performance, and economic parameters for potential future aircraft designs under different policy and technological scenarios[4]." The architecture of APMT is shown Figure 2.

---

[3] PARTNER web site, http://web.mit.edu/aeroastro/partner/projects/project3.html
[4] PARTNER web site, http://web.mit.edu/aeroastro/partner/projects/project14.html

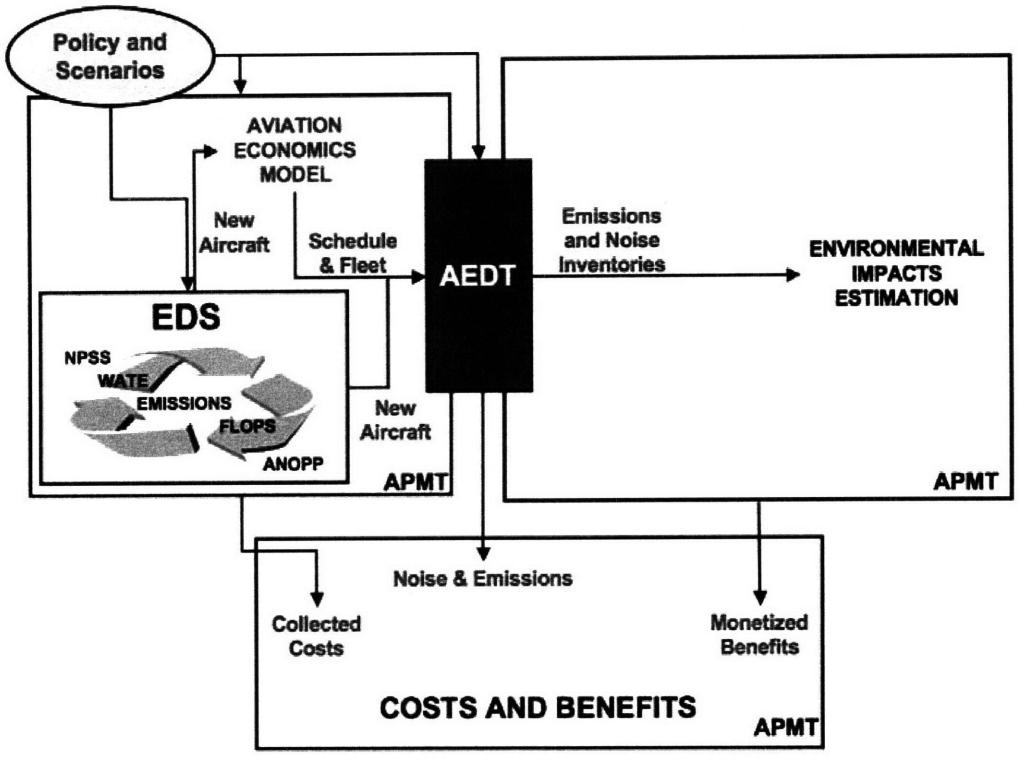


Figure 2 – APMT Architecture Overview[4].

1.2. Research motivation

In order to explore trade-offs among diverse future aircraft, EDS needs to assess fuel burn, emissions and noise for different aircraft designs. This thesis presents the development of a combustor model that computes NO_x, CO and soot emissions at sea level for use within EDS. Inputs to the model have to be chosen carefully, they must be convenient to use when projecting future technology and they must be relevant to combustor characteristics.

1.3. Emission Regulation

In order to control the amount of pollution from aircraft in the vicinity of airports, the International Civil Aviation Organization (ICAO) has implemented emission

standards for soot, unburned hydrocarbons (UHC), carbon monoxide (*CO*) and oxides of nitrogen (NO_x) that must be met by all subscribing countries. Except for soot, emission standards are defined for a Landing Take-Off cycle (LTO) cycle that defines the typical operations below 3,000 ft, i.e. near the airport. The LTO cycle comprises approach to the airport (30% Sea Level Static (SLS) thrust), idle (including taxi, equivalent to 7% SLS thrust) time, take-off (100% SLS thrust), and climb-out (85% SLS thrust). Figure 3 illustrates the four modes and the time spent in each mode (Time In Mode TIM).

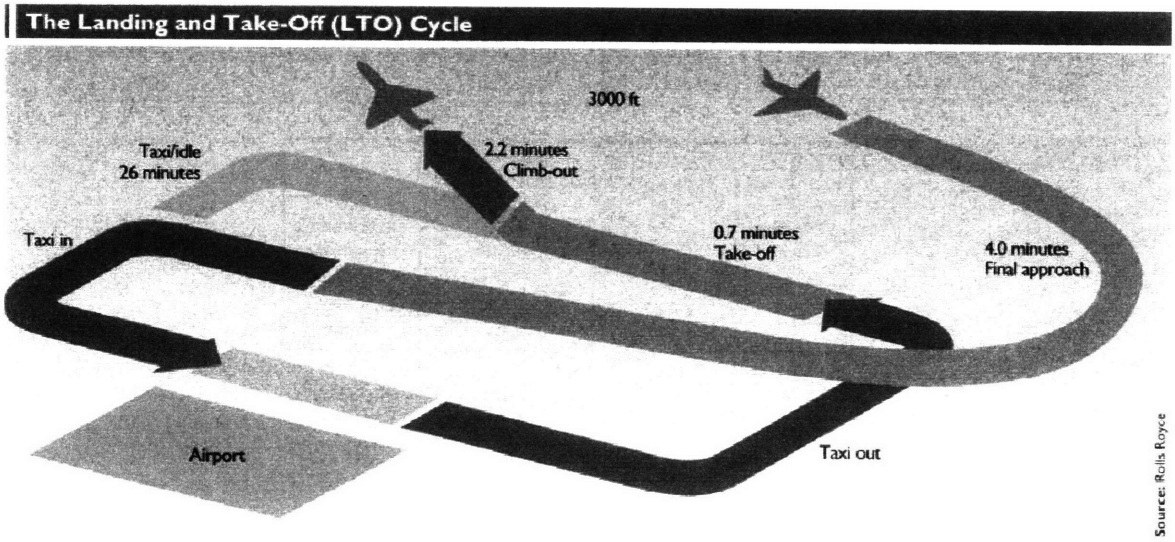


Figure 3 - Landing and Take-Off Cycle[5]

For NOx, CO and UHC emissions, the last regulation adopted to date[6] is based on the LTO emissions per unit thrust (Dp/Foo), defined as:

$$Dp/Foo = \frac{\sum_{i=1}^{4} EI_i \cdot TIM_i \cdot \dot{m}_{fi}}{RO}$$

where EI_i is the emission of pollutant in mode i, $\dot{m}_{fi}$ the fuel flow in mode i, and RO the rated output. Limits exist for each species, and are function of the certification date and of the rated output of the engine at sea level static conditions.

---

[5] P.J. Jeanniot, "Environmental Review," International Air Transport Association, ISBN 92-9035-732-0.
[6] ICAO Annex 16 Amendment 5 (November 24, 2005)

Regulation for soot is slightly different as it applies for all modes. The Smoke Number limit is:

$$SN_{max} = \min(50,\ 83.6 \cdot Foo^{-0.274})$$

where *Foo* is the rated thrust. This limit usually applies to the maximum power, take-off, since soot emissions typically increase monotonically with power (although some engines display more complicated behavior).

1.4. Smoke Number

Contrary to NO_x, , or *HC*, certification procedures do not measure the emission index (*EI*) for non-volatile particulate matter (soot). Instead, certification procedures evaluate smoke emissions using an indirect measurement of the smoke plume visibility of the engine. This method was implemented to eliminate the visible exhaust of aircraft, a major concern in the 1970's when the rules were first put in place. The measurement is done by positioning a filter at the exhaust of the engine that traps smoke particles contained in a given mass of exhaust gas. Then, the reflectance of the filter is measured and is compared to the reflectance of the paper before staining it. The comparison yields the Smoke Number (*SN*).

$$SN = 100 \cdot \left(1 - \frac{R_s}{R_w}\right)$$

R_s and R_w are the reflectance of respectively the stained filter and the unstained filter.

The bigger the smoke number is, the more soot is emitted. The uncertainty of such a measurement is high as it is estimated to be plus or minus 3 *SN*, to be compared to maximum *SN* values of usually less than 30, i.e. an uncertainty at least higher than 10%. More than 60% of engines have a smoke number below 10, so uncertainty is at least 30% in 60% of measurements.

1.5. Previous Work

The combustor model presented in this thesis was originally developed by Allaire as part of his Masters' thesis at MIT[7]. It predicts NO_x and CO emissions of current and potential future gas turbine engines within quantified uncertainty bounds. In achieving those objectives, the model needed to meet specific attributes including:

- Use of high level input variables such as the compressor exit temperature and pressure (T_3, P_3), combustor volume, and mass flows of air and fuel entering the combustor ($\dot{m}_{air}$ and $\dot{m}_{fuel}$). These inputs were determined to be convenient for an expert to use in projecting future technology.
- It should represent the physical relationships between operating conditions, input variables and pollutant emissions.
- The model must apply to any combustor technology so it can be used to assess emissions of future engines.
- Fast computation times are required relative to three-dimensional CFD computations.
- Uncertainty must be quantified through comparison to existing technology to the extent possible. Uncertainties approaching the measurement uncertainties for emissions indices for the active fleet are a goal, i.e. about 16% for NO_x and 23% for CO.

As shown by Allaire, the model meets those objectives for NO_x and CO emissions, and achieves particularly good prediction for NO_x emissions (model estimates are all within ±16% uncertainty with the exception of idle) for the small number of engines for which comparisons to experiment were presented. An overview of the combustor model is shown below:

---

[7] Douglas L. Allaire, "A Physics-Based Emissions Model for Aircraft Gas Turbine Combustors", Master's Thesis, Massachusetts Institute of Technology, 2006.

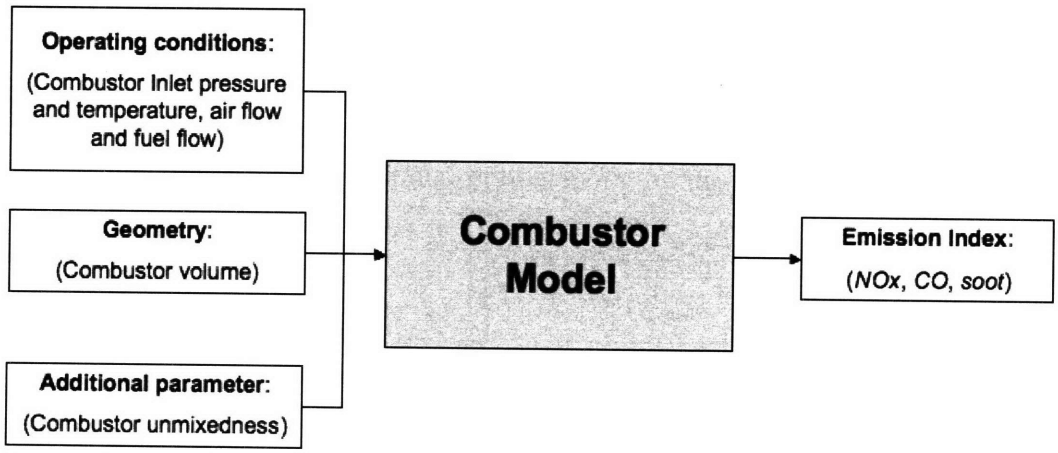


Figure 4 – Inputs and outputs of the combustor model

The model represents the physical layout of a combustor. It consists of a primary zone, an intermediate zone, and a dilution zone, that are modeled by either perfectly stirred reactors (PSR) or plug flow reactors as shown in Figure 5. PSRs are ideal reactors that assume instantaneous mixing. They are adequate to model combustion processes that have negligible characteristic mixing times relative to burning times. Plug flow reactors assume steady inviscid flow with ideal gas behavior and no mixing in the axial direction.

Primary zones of typical combustors have large recirculation regions of flow, high temperatures, and high levels of turbulence. Short characteristic mixing times relative to burning times are usually associated with high levels of turbulence, suggesting that PSRs are appropriate to model this region. 16 Parallel PSRs – each PSR has a different fuel-to-air ratio – capture the unmixedness of air and fuel in the primary zone associated with the injection of fuel inside the combustor.

The intermediate zone's role is to slowly add dilution and cooling air while maintaining a high enough temperature to complete combustion. It also serves as an extension of the primary zone to burn pockets of fuel-rich mixture when they exist. Testing revealed that a single plug reactor provided the best results for the intermediate zone.

The dilution zone is designed to cool down the gas to an acceptable mean temperature and to improve the pattern factor prior to the turbine inlet. The flow is essentially one-

dimensional and is therefore reasonably well modeled by plug flow reactors. Two serial plug flow reactors are used to model this region, divided by the addition cooling air between both plugs.

Finally, dilution and cooling air are modeled through the addition of air between each zone.

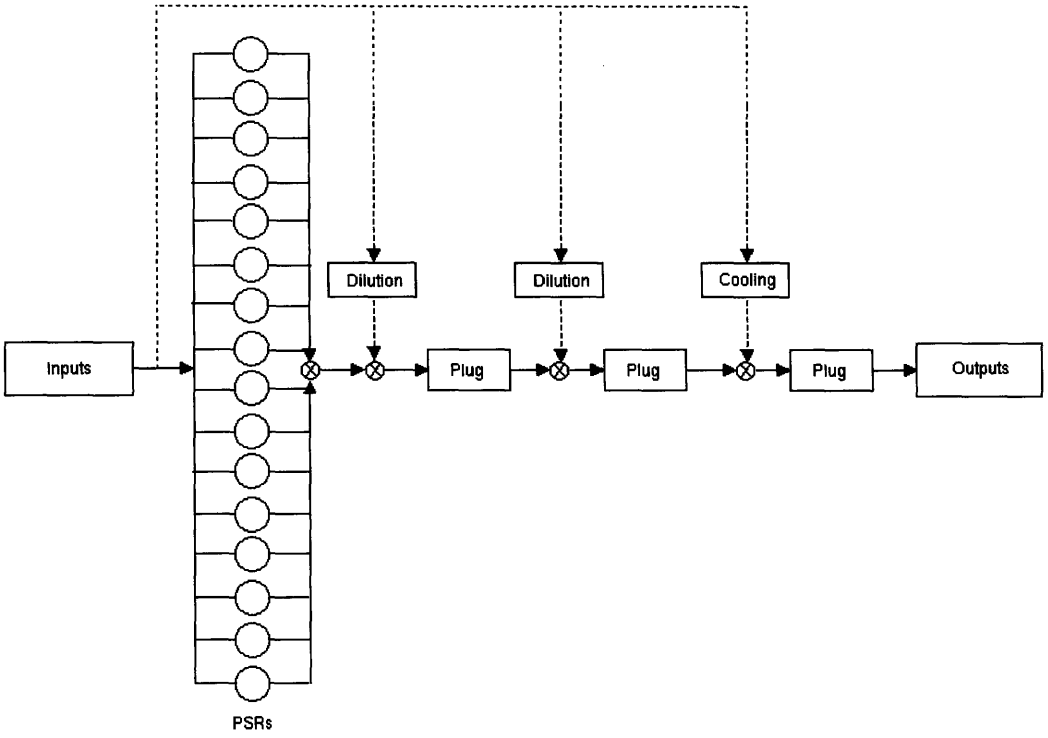


Figure 5 – Schematic of Allaire's network reactor model[7]

1.6. Thesis Objective

The objective of the thesis is to develop a soot emissions model for use in the combustor model previously developed by Allaire for EDS. The soot model must meet the same attributes as the previous version (see paragraph 1.5). Soot emissions are historically the most challenging to predict of the major pollutant emissions. They are very sensitive to design and operating parameters. The first objective is to represent the trend of soot emissions for the 4 ICAO LTO cycle modes (idle, approach, climb-out and

take-off). This trend is different for all engines, but takeoff smoke number is usually the largest value. Two engines that have different trends are modeled in this thesis: the PW4090 engine and the CFM56-2C engine. If the trend objective is met, the next milestone is to generate soot emissions estimates for other engines in the fleet.

1.7. Organization of the Thesis

The thesis describes and analyzes the soot formation mechanisms that are implemented in the combustor model.

Chapter 2 defines particulate matter (PM), describes the health and environmental problems associated with PM, and details the current methodology to assess PM emission in engines exhaust. Chapter 3 describes the soot properties and the formation mechanism of soot, setting the modeling equations to be used. Chapter 4 explains how the soot mechanism was implemented in the combustor model, and finally Chapter 5 discusses the results obtained.

Chapter 2

Particulate Matter (PM)

This chapter describes the typical particulate matter (PM) that is found in the exhaust of aircraft engines. Different types of particulate matter are listed, classified, and the impacts on health and climate change are described. Finally, the current method used by FAA and EPA to estimate PM emissions (FOA 3.0) is described. The method will be used later on to compare the emission indexes generated by the combustor model to the ICAO emission indexes.

2.1. Definition and Classification

Particle matter (PM) is not classified as specific species or as a specific chemical group like nitrogen oxides, alkanes or alkenes are for instance, but as a mixture of small particles and liquid droplets. PM is made up of various components, like acids, organic chemicals, metals, and dust particles, and can contain hundreds of chemical components. Typical PM types are dust, dirt, soot, smoke, and liquid droplets emitted by factories or combustion engines.[8] Typical PM emitted by aircraft engines include soot, lube oil, fuel organics and sulfates.

PM can be composed of volatile particles, non-volatile particles, or non-volatile particles coated with liquid. In aircraft engines, volatile particles are composed of fuel organics, lubrication oil and fuel sulfur, and non-volatile particles are soot particles (black carbon). Other classifications apply and are presented below; they take into account the size of the particles or how they are formed.

[8] EPA web site

Size distribution

The "inhalable coarse particles" category (referred to as PM_{10}), contains particles whose diameter is larger than 2.5 micrometers and smaller than 10 micrometers. These particles are usually found near roadways and dusty industries. The second category contains "fine particles", particles whose diameter is less than 2.5 micrometers. They are referred to as $PM_{2.5}$. Such particles can be emitted from forest fires, combustion engines, or by subsequent reactions from gases emitted by power plants, industries or engines.

Reaction pathway

Researchers also differentiate particles emitted directly in the air by the pollutant source (primary particles) from the ones that are subsequently formed from complicated reactions between the combustion gases released and other chemical species in the atmosphere (secondary particles).

Aircraft Particulate Matter

Studies have shown that both non-volatile and volatile particulate matter is found in the exhaust of aircraft engines. Non-volatile particles form in the hottest areas of the combustor and in the early part of the turbine. No subsequent reaction occurs in the atmosphere; they are listed as primary particles.

Volatile particulate matter can be either primary or secondary PM. For instance, fuel sulfur particles emitted are largely composed of secondary particles; they mix in the atmosphere and react to form ammonium sulfates. The same is true of ammonium nitrate PM which is typically formed from precursor gases of NO_x. Oil particulate matter, on the other hand, originates from leaks in the engine and do not evolve once in the atmosphere; they are primary particles. Finally, a good approximation is that particulate matter emitted by aircraft all belongs to the $PM_{2.5}$ category[9].

Major PM found in aircraft exhaust are listed Table 1.

---

[9] Derivation of A First Order Approximation of Particulate Matter From Aircraft, Paper # 69970, Roger L. Wayson, Gregg G. Fleming, Brian Kim and Julie Draper

Non-volatile PM	Volatile PM
Soot (C_s)	Fuel Sulfur (SO_x)
Some metals	Fuel Organics
–	Lube oil (can be included in fuel organics as well)

Table 1 – Major PM compounds found in aircraft exhaust.

2.2. Health and Climate Issues Related to PM

There is a well established correlation between exposure to particulate matter and adverse health effects. Particulate matter hazards come from both their size and their chemistry. Their size allows them to enter the lungs where chemicals may diffuse into the blood through the gaseous exchange in the lungs and can cause cardiovascular effects. The smallest particles are estimated to have the strongest adverse health impacts[10]. They increase the risk of lung cancer, and may contribute to thousands of premature deaths each year. Illnesses related to PM include new cases of chronic bronchitis, and aggravation of existing respiratory and cardiovascular disease.

In addition to health problems, PM contributes to global climate change. Sulfate aerosols intercept incoming sunlight and reduce the energy flux arriving to the Earth's surface[11]. Soot has a slightly different effect as it absorbs light and influences clouds, meaning it warms up the atmosphere (due to light absorption) and cools down the surface (by reducing energy flux reaching it). Besides, it acts as a seed for water condensation. Water droplets are then bigger than usual, making the cloud denser and reflecting more solar radiation. The result increases the effect of warming the atmosphere and cooling the surface.

[10] European Commission, 2005
[11] Charlson, R. J. et al. Climate forcing by anthropogenic aerosols. Science 255, 423-430 (1992)

2.3. Measurement of Non-Volatile PM for Aircraft Engines

Measurement of soot emissions for aircraft engine is done by measurement of the Smoke Number. The method may be used to estimate of non-volatile particulate matter, but development of additional measurements is necessary. First, Smoke Number measurements do not meet high levels of precision, as uncertainties are usually around 30%. Further, the method does not capture some of the important physical characteristics of emitted particles, such as the soot mass flow and the particle size distribution. Two engines can have similar smoke numbers and have different mass flow rates of soot emissions. Over the last 10 years, people have proposed to include more accurate data during the certification measurements. For instance, it has been recommended that mass flow and size distribution be recorded[12] instead of only Smoke Number. This would give more meaningful data and would provide researchers with better data to work with, but it requires more complex measurements. Research is currently on-going by groups such as the Society of Automotive Engineers (SAE) to standardize measurement techniques for aircraft PM, but it will not be completed for years to come. Even after acceptance of a standard method it will be additional years before certificated measurements are achieved and validated and a fleet database is completed.

The FOA Method

Because engine certification still requires measurement of Smoke Number only, a method has been created to assess mass flow emissions of the different types of particulate matter based on SN measurements. This method is called First Order Approximation (FOA) (see Appendix A). As it is stated in the document, "this method is approximate and is only to be considered an interim approach until measured, statistically valid data are available[9]." The FOA method is based on studies that showed correlation between the reported smoke number and mass emissions. FOA relies on the assumptions

[12] Steve Lukachko's PhD thesis, MIT

that the change in mass emissions is correlated to the change in SN[13] and that the few data that are accessible are representative of commercial aircraft. A relation between mass emissions and SN is then extrapolated. The last released version is version 3.0. It is different from version 2.0 in the sense that non-volatile and volatile PMs are not correlated anymore. In version 2.0, volatile PMs were obtained by multiplying non-volatile PM (obtained using a direct relationship with SN) by a factor of 3. In version 3.0, each volatile component is also assessed independently of others. More details are found Appendix A.

In order to estimate soot emission indices from the ICAO Smoke Number, FOA3.0 introduces the concentration index CI (mg/m^3) and the core exhaust volume per mass of fuel Q (in $M^3/kg\ fuel$). Regression is made between CI and SN, and standard Q is estimated for the 4 ICAO points. The product $Q \cdot CI$ yields the emission index. More precisely, the method introduces different regression functions for SN below and above 30 that account for technology, as most modern engines have a smoke number below 30 whereas older engines' Smoke Numbers are usually above 30.

Based on regression of the data, the relation between concentration of soot CI (Concentration Index, expressed in mg/M^3) and Smoke Number SN is:

$$CI = 0.0694(SN)^{1.23357} \qquad \text{for } SN \leq 30$$

$$CI = 0.0297(SN)^2 - 1.802(SN) + 31.94 \qquad \text{for } SN > 30$$

Concerning the determination of Q, the FOA method assumes that average air-to-fuel ratios (AFR) per power settings can be assumed for all commercial turbine jet aircrafts[14] (see Table 2).

---

[13] Based on the findings of Wayson, R.L., G. Fleming, B. Kim, in A Review of Literature on Particulate Matter Emissions from Aircraft, DTS-34-FA22A-LR1, Federal Aviation Administration, Office of Environment and Energy, Washington, D.C. 20591, December, 2003

[14] Eyers, C., CAEP/WG3/AEMTG/WP5, Improving the First Order Approximation (FOA) for Characterizing Particulate Matter Emissions from Aircraft Engines, Alternative Emissions Methodology Task Group (AEMTG) Meeting, Rio De Janeiro, Brazil

Power Setting	AFR
7% (idle)	106
30% (approach)	83
85% (climbout)	51
100% (takeoff)	45

Table 2 – Assumed air-to-fuel ratios by power setting

The core exhaust volume per mass of fuel (Q) is calculated as:

$$Q = 0.776 \cdot AFR + 0.733$$

$$\text{or} \quad Q = (0.776 \cdot AFR + 0.733)(1 + \beta)$$

in the case Smoke Number is measured with bypass air (bypass ratio is β) as would be the case for internally mixed turbofan core and bypass streams.

Engines modeled in this thesis are relatively modern and have a Smoke Number less than 30. Their smoke number has also been measured without bypass air so we will use the following equation as the soot reference function in the model, as well as ICAO SN.

$$\boxed{EI_{non-vol} = 0.0694 \cdot SN^{1.23357} \cdot (0.776 \cdot AFR + 0.733)}.$$

Chapter 3

Soot Formation

Soot is the most prevalent non-volatile particulate matter found in aircraft engines. Other compounds such as metal particles are negligible and non-volatile PM emissions are considered to be soot only. Soot emissions originate due to incomplete combustion of hydrocarbon fuels and their formation occurs in the hottest parts of the flame, where fuel and air are poorly mixed. Soot size, shape, and the complex conditions necessary for its formation, make soot formation difficult to study. It has received considerable interest in the last 40 years and knowledge has significantly increased. However, there are still unanswered questions, especially for the turbulent high-pressure flames typical of aircraft gas turbine combustors. This chapter describes the current knowledge of soot properties and soot formation, and details the current best mechanism rates that model soot behavior.

3.1. Soot Properties

Soot, or black carbon, is made almost entirely of carbon. Other species such as hydrogen or oxygen or nitrogen can be found, but in low quantities. Typical ratios[15] of C/[i] are 8.3 to 18.3 for i=H, 58 to 109 for i=O and 292 to 976 for i=N.

Soot particles almost never exceed 1μm so soot belongs to the $PM_{2.5}$ category. Figure 6 shows typical shapes of soot particles. They are aggregates of nearly spherical carbon primary particles having relatively uniform diameters. They also exhibit fractal behaviors with a mass fractal dimension below 2.

---

[15] Combustion Science and Technology, Vol. 108, Nos. 4-6, 1995, pp. 207-229, Faeth, G.M., and Koylu, U.O., "Soot Morphology and Optical Properties of Nonpremixed Turbulent Flame-Environments,"

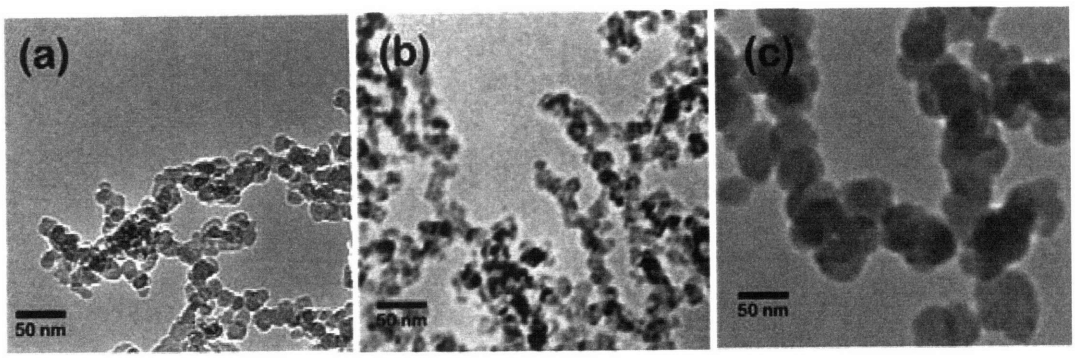


Figure 6 - TEM photographs of soot aggregates at maximum soot volume fraction location along the axis of different flames, showing the texture of soot particles[16]

For long combustor residence times, primary particles are well modeled by a Gaussian distribution with mean primary diameter just below 60 nm and standard deviation smaller than 25%[17]. The size distribution of the particle aggregates is appropriately modeled by a lognormal Gaussian distribution with an average size and a standard deviation that depend on the residence time. Those aggregates subsequently cluster to each other and form bigger open structured particles. As time elapses, soot particles do not look like primary particles touching each other anymore, but more like spherical particles that would have merged together because of soot growth.

Chemical properties like density, porosity are similar to black carbon. It is therefore a good estimate to assume a density of 1820 kg/m^3, and this value will be used later. Also similar to carbon is the structure of primary particles composing soot. They consist of carbon layers, like graphite. Such a structure is shown Figure 7.

---

[16] 44th AIAA Aerospace Sciences Meeting and Exhibit, Soot Formation and Oxidation in Laminar Flames, from C. H. Kim, F. Xu, P. B. Sunderland, A. M. El-Leathy and G. M. Faeth

[17] AIAA2001-03ZZ, Soot Research in Combustion Science: Introduction and Review of Current Work from D. L. Urban and G. M. Faeth



Figure 7 - Structure of a soot primary particle[18]

3.2. Soot Formation Pathway in Aircraft Combustors

As mentioned before, soot is produced in the hottest parts of the combustor, in the fuel-rich regions and in the early stages of the turbine[19]. However, for new engines with better mixing of air and fuel, soot formation is reduced and almost no soot is created in the turbine. Based on the work of Dakhel P. M. and Waitz I. A.[20], it has been shown that PMs do not evolve significantly in the plume of aircraft engines, and soot is considered a primary PM. In addition, time spent in the high-pressure turbine (HPT) is relatively low compared to the time spent in the combustor, so oxidation in the HPT affects little if any soot particles. Finally, temperature in the low-pressure turbine is too low to affect soot so the mass of soot exiting the engine is the same as the mass of soot exiting the combustor. For these reasons, we consider mass emissions of non-volatile PMs recorded from engines to come from the combustor, and the model objective is to match those values.

---

[18] From The Evolution of Soot Precursor Particles in a Diffusion Flame, from Dobbins et al. (1998) p. 286, Vol. 115, Combustion and Flame, Combustion Institute

[19] Energy Combustion Sci. Vol. 23, Models of Soot Formation and Oxidation, Ian M. Kennedy

[20] Pierre M. Dakhel, "Modeling of Particulate Matter Creation and Evolution in Aircraft Engines, Plumes and Particle Sampling Systems", Master's Thesis, Massachusetts Institute of Technology, 2005.

Soot radiation is both a strength and it is problematic. It is a strength because it makes spotting of soot easier, as the flame gets a bright yellow color and makes optical measurements of soot concentration possible. The drawback from a modeling standpoint is its complexity. Unlike other species such as NO_x, soot depends heavily on the flame structure. Soot has influence on the flame as it releases heat through radiation, and understanding soot formation requires taking this feedback effect into account. This feature is responsible for the lack of modeling and understanding on soot formation. Many efforts have been undertaken over the last few years to understand the mechanisms of soot formation in engines. Progress has been made, but there are many questions that remain unanswered concerning each stage of the soot evolution (nucleation, growth, oxidation and coagulation). For aircraft engines, radiation of soot makes hardware life and durability of engines – especially durability of combustor liners – decrease because flame temperature increases with flame radiation. It also reduces efficiency of the engine and increases fuel consumption, but these effects are relatively insignificant.

3.2.1. Precursors

The soot formation path can be described as follows: particles react to form bigger chemical compounds, then grow, then collide with one another to form incipient soot particles, and finally grow, coalesce and get oxidized. The early compounds that trigger this path are called soot precursors. Over the years, many species have been thought of being a precursor to soot. Inceptions of polyacetylenes, ionic species, or polycyclic aromatics hydrocarbons (PAHs) were all once considered to be the key elements for soot nucleation. As of now, it is considered that the first two listed species are not crucial to soot formation, and that soot is obtained through PAHs[21].

Polycyclic Aromatic Hydrocarbons (PAHs)

PAHs are chemical compounds that contain at least two simple aromatic rings bonded together, and that have neither heteroatoms (atoms other than C and H) nor substituents. Even though naphthalene ($C_{10}H_8$) fits into the definition, it is not a PAH by convention.

[21] PCCP, Reaction mechanism of soot formation in flames, Michael Frenklach

Anthracene ($C_{14}H_{10}$) is one of the simplest PAHs. Table 3 lists some of the simplest PAHs along with their formula and shape.

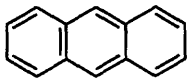
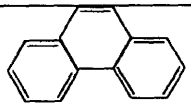
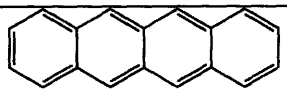
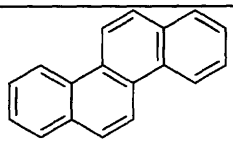
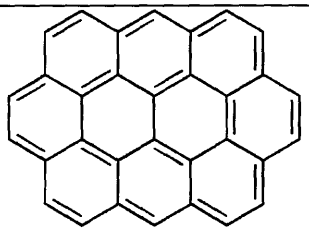
PAH's name	Formula	Shape
Anthracene	$C_{14}H_{10}$	
Phenanthrene	$C_{14}H_{10}$	
Naphthacene	$C_{18}H_{12}$	
Chrysene	$C_{18}H_{12}$	
Ovalene	$C_{32}H_{14}$	

Table 3 - Examples of simple PAHs[22]

PAHs are also considered organic pollutants and affect air quality as some of them are carcinogens and others trigger health problems. As they are emitted with soot, they contribute to the health issues associated with soot emissions. They are due to incomplete combustion of crude oil, kerosene, or other compounds. PAHs can have as many rings, but few of them reach more than seven rings as they become large and unstable. The most commonly found PAHs have five or six rings.

The presence of aromatics in the fuel leads to higher soot creation rates since formation of the first aromatics ring – which is the rate-limiting step in the formation of PAHs (see paragraph 3.3.1) – can be bypassed. Legislation requires that fuels used for

[22] Table inspired from http://en.wikipedia.org/wiki/Polycyclic_aromatic_hydrocarbon

civil air transportation have less than 22% volume of aromatics[23]. An ideal value would be zero but the proportion of aromatics is too high to economically justify their removal. Figure 8 addresses the importance of the fuel surrogate that will be used in the model. As smoke depends on both aromatics content and hydrogen content, it is important to use a fuel surrogate that is similar to Jet A as far as soot is concerned.

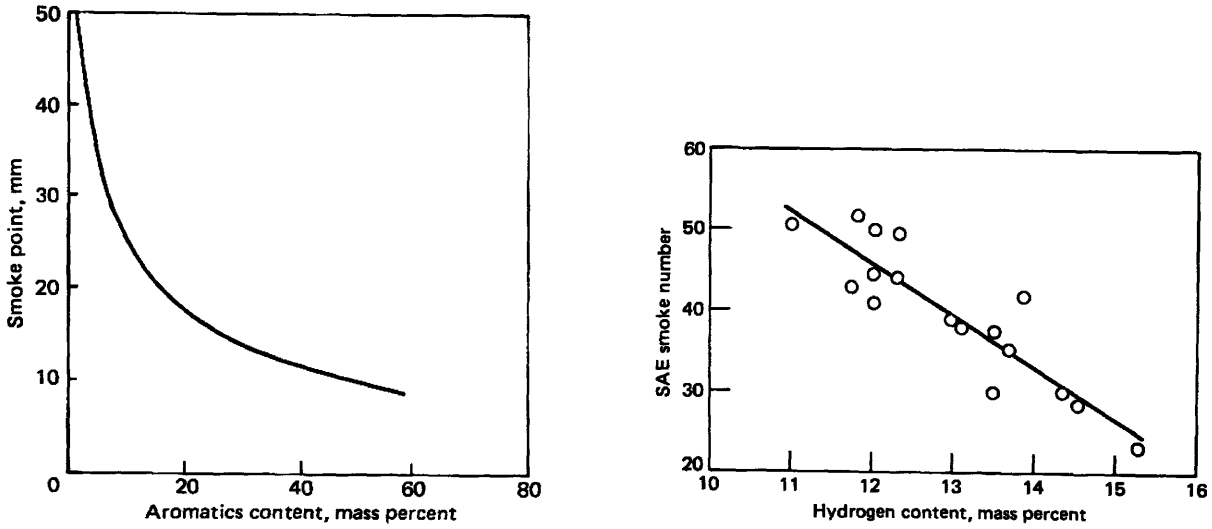


Figure 8 – Sooting effects of aromatics and hydrogen fuel content (from A. Lefebvre, Gas Turbine Combustion)

	Kerosene
Equivalent for U.S. civil	Jet A; Jet A-1
Aromatics (by volume)	22%
Olefins (by volume)	5%
Sulfur (by mass)	0.3%

Table 4 - Representative Chemical Limits for Aircraft fuels[24]

[23] Toxicologic Assessment of Jet-Propulsion Fuel 8 (2003), http://books.nap.edu/openbook.php?record_id=10578&page=9

[24] Gas Turbine Combustion, Arthur Lefebvre

3.2.2. Nucleation

Soot undergoes 4 types of reaction while in the combustor. The first one is nucleation and is described below. After incipient soot particles are formed, they grow, get oxidized and coagulate before exiting the combustor. Each reaction affects either the mass of soot or the number of particles, or both. For instance, nucleation creates new particles so it changes both mass and particle densities. Growth and oxidation, on the other hand, affect only mass, and coagulation affects only particle densities.

As mentioned above, the current understanding is that PAHs (polycyclic aromatic hydrocarbons) are the principal species responsible of soot nucleation[18]. In this nucleation process, the first step towards PAH is the formation of the first aromatic ring from hydrocarbons present in fuel. This step is highly important because it is considered to be the rate limiting reaction for PAH formation. As a consequence, it controls the rate of PAH formation and subsequently controls the rate of soot nucleation.

Once the first aromatic is created, primarily C_5H_5, growth of the soot precursors (PAHs) follows an HACA mechanism[21]. This mechanism is detailed paragraph 3.3.2**Error! Reference source not found.**; aromatics need to be activated, then acetylene radicals cluster to the activated molecule and make aromatics grow. More precisely, H molecules convert the aromatics to their radicals (activation) and acetylene bonds to the radicals (growth).

When they are large enough, PAHs are able to stick to each other by collision: their sizes increase. They create PAH dimers, then collide with simple PAHs to form trimers, then form tetramers and so on and keep growing through collisions. This process makes the PAHs evolve from gaseous species to solid particles, the first "solid particle" being usually assumed to be a dimer. The incipient soot particle is formed.

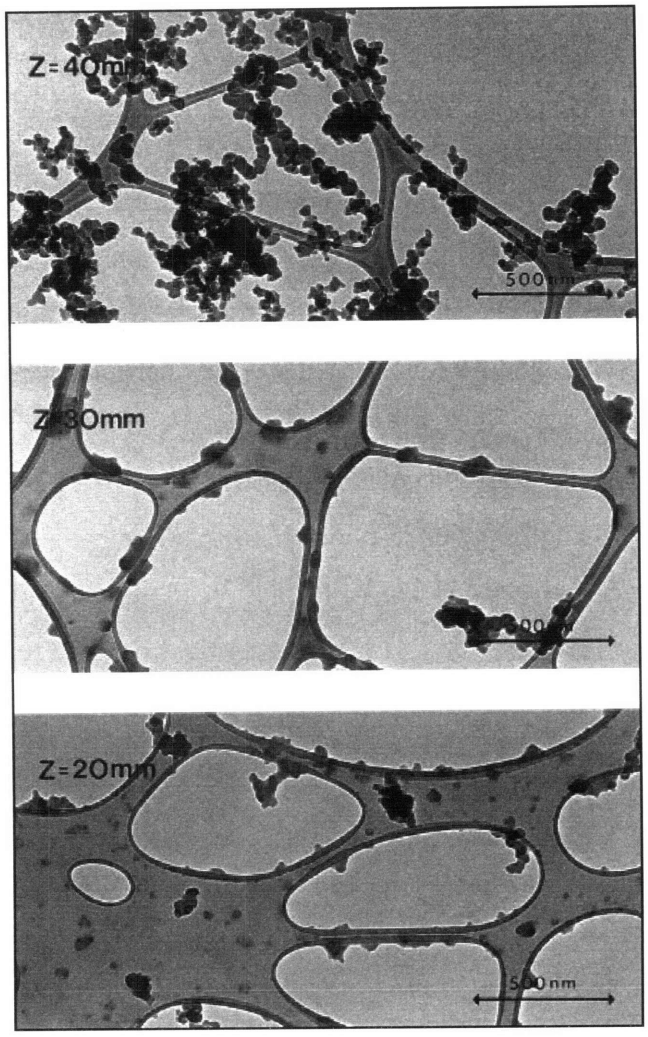


Figure 9 – Micrographs of soot particles captured on carbon grids, from an ethene diffusion flame. The transition from precursor particles to soot aggregates occurs between Z = 30 and 40 mm [25]

3.2.3. Growth, Oxidation, and Coagulation

Once the incipient soot particle is formed, growth, oxidation and particle coagulation change the physical characteristics of the initial soot particle. Typical chemical mechanisms are HACA for soot surface growth, and O_2 or OH oxidation for soot oxidation. Studies have also shown that in typical flames, growth and oxidation rates are much higher than nucleation rates.

---

[25] From The Evolution of Soot Precursor Particles in a Diffusion Flame, from Dobbins et al. (1998) p. 286, Vol. 115, Combustion and Flame, Combustion Institute

b. photograph near the maximum soot concentration condition (z = 50 mm);

c. photograph near the end of soot surface oxidization (z = 70 mm).

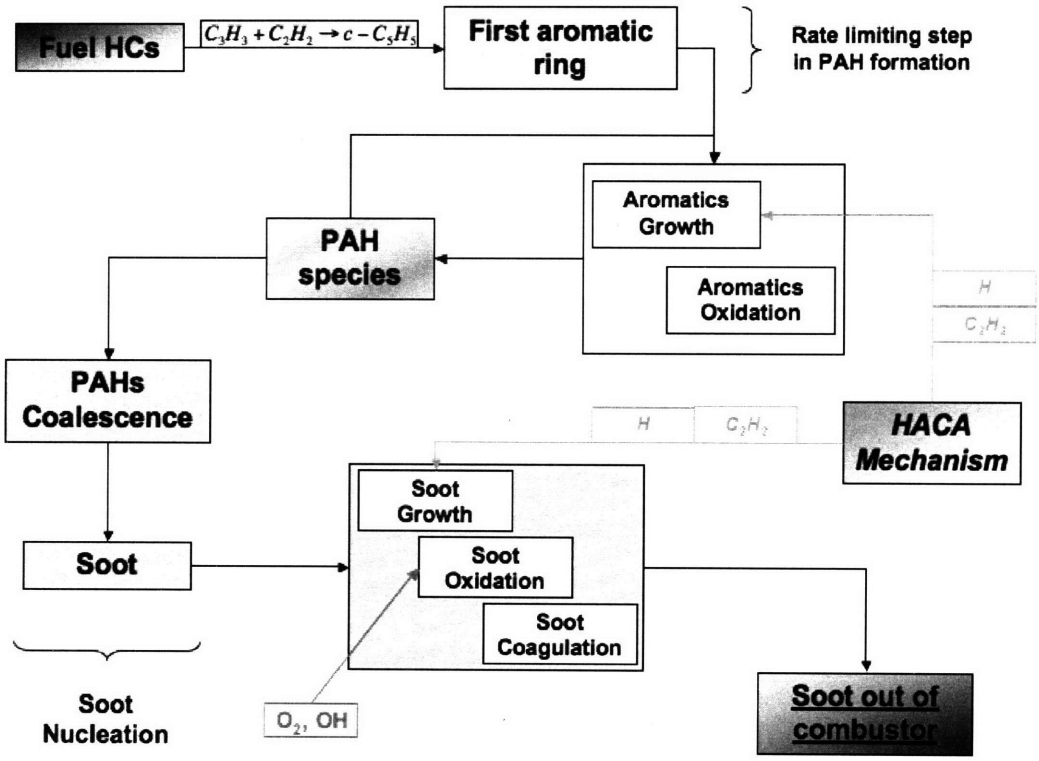


Figure 11 – Soot formation path

3.3. Modeling Rates of Soot Formation inside the Combustor

Based on the soot creation path described above, different models have been proposed. Lindsted was the first one to propose a model that could accurately predict soot emissions for a wide range of conditions[27]. The model is based on acetylene for growth and nucleation, and *OH* for oxidation[28]. This model is described in reference [28]. He remarked that soot was less reactive in the latest part of the growth, and he

[27] Combustion and Flame (1991), 87 289-305, A Simplified Reaction Mechanism for Soot Formation in Nonpremixed Flames, K. M. Leung and R. P. Lindstedt

[28] Proceedings of the Combustion Institute (2007), J.B. Moss, I.M. Aksit, Modelling soot formation in a laminar diffusion, doi:10.1016/j.proci.2006.07.016

To sum up, hydrocarbons in the fuel react to form simple aromatic rings. After this initial reaction, aromatic rings react to form more complex rings and finally form PAHs. PAHs, when large enough, are solid and account for the incipient soot particles. Soot particles then undergo growth, oxidation and coagulation reactions in the combustors. Soot generally comes out of the combustor in an agglomerated form[26] and then does not undergo additional chemical reactions. The following figures outline the typical shapes and growth of soot particles and the typical path for soot creation inside an aircraft combustor.

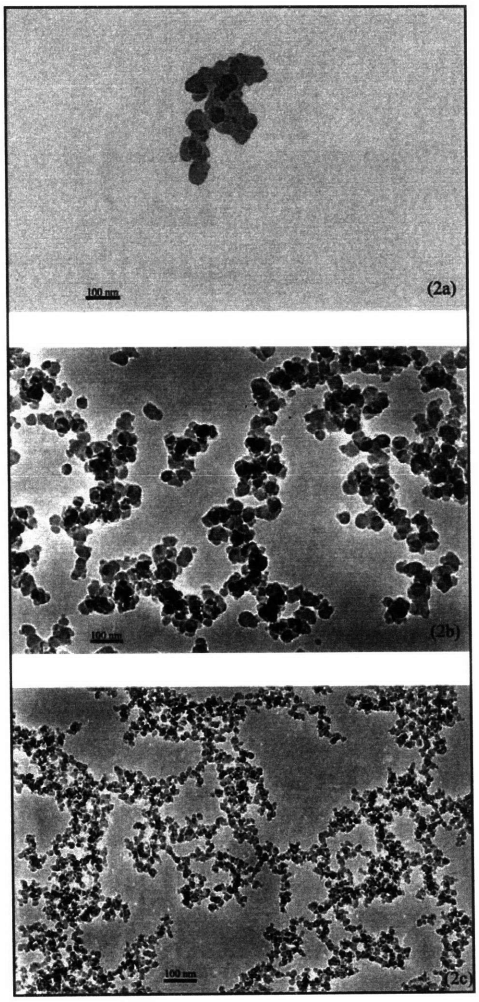


Figure 10 – Typical TEM photographs of soot aggregates along the axis of the ethylene-fueled laminar jet diffusion flame burning in air at atmospheric pressure[38]:
a. photograph near start of soot formation (z = 20 mm);

[26] Energy Combust. Sci., Models of Soot Formation and Oxidation, Ian M. Kennedy

suggested that the growth term should be modified to account for particle aging. Subsequent analysis showed that lower reactivity was not due to aging, but to a lack of reactivity of the particle. Soot must be activated by hydrogen before growing and follows a HACA mechanism. Still, due to the fact that it does not use radical species, Lindstedt's growth and nucleation models are still widely used. We describe both HACA and Lindstedt's models in this section.

3.3.1. Nucleation

Early Stages, Formation of Aromatics

This step is the least understood of all steps as many complex chemical species are thought to play an important role, as well as many reactions. There is also the difficulty of knowing when to consider a molecule solid and which first species is considered soot. Particles' sizes are also very small and require high optic resolution to observe them. As it has been seen, the current knowledge is that soot is created by aggregation of polycyclic aromatic hydrocarbons (PAHs).

The formation of the first aromatics ring plays a major role in the nucleation of soot as this reaction is considered to be the rate-limiting step in the reaction sequence to larger aromatics. In the last years attention has been given to this reaction in order to understand the soot formation pathway. Many initial pathways have been suggested to be the first step toward soot[21]. Researchers used either propargyl (C_3H_3) or acetylene as reactants because propargyl is extremely stable and acetylene is abundant in hydrocarbon fuel and is considered to play a major role in building up hydrocarbons. Reactions like (1), (2) and (3) were once proposed but were dismissed by subsequent analysis.

$$n-C_4H_3 + C_2H_2 \rightarrow phenyl \quad (1)$$

$$n-C_4H_5 + C_2H_2 \rightarrow benzene + H \quad (2)$$

$$C_3H_3 + C_3H_3 \rightarrow benzene \ or \ phenyl + H \quad (3)$$

Finally, a pathway relying on both propargyl radical and acetylene has been suggested and has proved satisfying, resulting in the following reaction:

$$\boxed{C_3H_3 + C_2H_2 \rightarrow c - C_5H_5} \quad (4)$$

Following its formation, cyclopentadienyl ($c - C_5H_5$) reacts rapidly to form benzene. Recent studies have shown the feasibility of this reaction and have determined the reaction rate is expected to be 2 to 10^3 faster than reaction (3)[21]. This property, when added to the fact that both propargyl and acetylene – stability and abundance – appear as reacting species, makes this reaction likely to play a key role in the formation of the first aromatic ring.

As a result, the first aromatics kinetic step is proportional to both propargyl and acetylene concentrations.

Nucleation: Growth of Aromatics, the HACA Mechanism

Aromatics growth can be described as a repetitive sequence of two principal steps. If we note A_i an aromatic chain, its growth occurs as follows:

- Abstraction of an atom of hydrogen from the aromatic chain:

$$A_i + H \Leftrightarrow A_{i^-} + H_2 \qquad \text{(HACA 1)}$$

- Addition of acetylene:

$$A_{i^-} + C_2H_2 \Leftrightarrow A_{i+1} + products \quad \text{(HACA 2)}$$

This mechanism is referred to as the HACA mechanism. HACA is an acronym for "H-abstraction, C_2H_2-addition". The abstraction step activates the aromatic by converting it to a radical A_{i^-}, which reacts with C_2H_2 to form a bigger aromatic. Aromatics activation can be achieved through different ways and by different species, but experimental data have shown that the abstraction by a gaseous H is the dominant reaction. Aromatics growth can also be achieved with species other than acetylene, but studies showed that the different pathways rapidly relax to the HACA mechanism.

The key feature of both reactions is reversibility[21]. Reverse reactions control the rate of aromatics growth and both reactions can be highly reversible. In many cases the second step reaction is extremely reversible and growth occurs – irreversibility occurs –

only when the aromatic formed is extremely stable because the system recovers entropy and decreases its energy. Coupling between (HACA 1) and (HACA 2) kinetics and stability of the products is what defines the HACA mechanism.

When HACA 2 is irreversible and HACA 1 is in equilibrium state, we get:

$$\frac{d[A_{i+1}]}{dt} = k_2 \cdot K_1 \cdot \frac{[H] \cdot [C_2H_2]}{[H_2]} \cdot [A_i]$$

where K_1 is the equilibrium constant of reaction HACA 1 and k_2 is the reaction rate coefficient of reaction HACA 2.

In most flame conditions, growth rate is proportional to acetylene concentration, as well as the reaction rate of the first aromatics ring. Combination of both reactions makes the overall nucleation rate proportional to $[C_2H_2]$. It is the reason why HACA and Lindstedt's nucleation model rates are proportional to acetylene.

The HACA mechanism goes further as it inferred from the previous equation that the nucleation rate is proportional to $[H]$ as well. But correlation with data is limited as seen Figure 12.

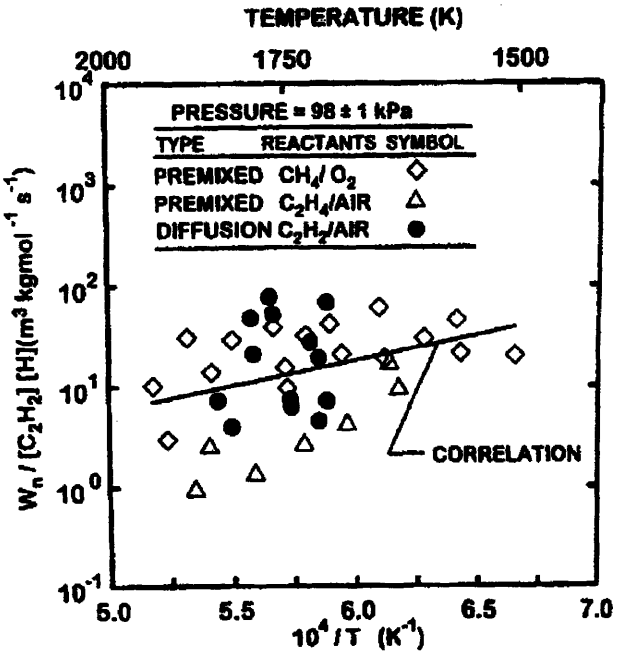


Figure 12 – Nucleation energy activation estimation for HACA model for laminar premixed and diffusion flames[17]

For the model proposed by Lindstedt, $w_n / [C_2H_2]$ is considered to be a function of temperature only. By correlating the data to the model, Lindstedt obtained a nucleation rate[28] $w_n = a.M_P[C_2H_2]e^{-21,000/T}$, with a = 54 s^{-1} and $M_P \in$ [144 ; 2000] kg/kmol. M_P represents the mass of an incipient soot particle and depends on the number of atoms in the particle.

3.3.2. Growth: HACA Soot Particle Surface Mechanism

There are many similarities between soot surface and PAHs. Based on that remark, people have shown that soot growth is proportional to acetylene concentration (Lindstedt's model) and that it might follow the HACA mechanism. Two different HACA soot growth paths are presented in this section.

The first model is due to Frenklach and co-workers[29] and is noted *FW*, the second one has been established by Colket and Hall and is noted *CH*[30]. These mechanisms are described Table 5 and Table 6. The mass growth rate of each mechanism is noted R_i, with i = *FW* or *CH*, and the net growth rate per unit of soot area is noted w_g. The relation between soot growth rate and each mass growth mechanism is defined as $w_g = \alpha_i.R_i$, with *i=FW* or *CH*. α_i is an empirical factor, closed to unity, which models the difference between soot sites and the final compound of any mechanism. The underlying idea is that chemical reactions taking place on the surface of soot particles are analogous to those on large PAHs. The soot surface is considered to be like the edge of large PAHs, covered with C-H bonds21 and growth follows a HACA mechanism. The main difference with PAH is that soot sites are not gaseous, so the empirical factor is different from 1.

The principal difference between both mechanisms is that one (FW) involves fewer reactions than the other, but has an empirical factor that is a function of the maximum

---

[29] Kazakov, A., Wang, H., and Frenklach, M., Combust. Flame 100:111 (1995).
[30] Colket, M. B., and Hall, R. J., in Soot Formation in Combustion (H. Bockhorn, Ed.), Springer-Verlag, Berlin, 1994, p. 442.

temperature of the flame, while CH's empirical factor is a constant. Both mechanisms show very good correlations for different conditions and flames.

Reaction Mechanism from Colket and Hall[30]

Reaction number	Reaction	A (m, kg mol, s)	E (kJ/(kg.mol)
1	$C_s - H + H \rightarrow C_s\bullet + H_2$	$2.5*10^{11}$	50,200
-1	$C_s\bullet + H_2 \rightarrow C_s - H + H$	$4.0*10^{8}$	29,300
2	$C_s\bullet + H \rightarrow C_s - H$	$2.2*10^{11}$	_
-2	$C_s - H \rightarrow C_s\bullet + H$	$2.0*10^{17}$	456,000
3	$C_s\bullet + C_2H_2 \rightarrow products$	$3.0*10^{14}$	259,000
4	$C_s\bullet + C_2H_2 \rightarrow C_sCH\dot{C}H$	$2.0*10^{9}$	16,700
-4	$C_sCH\dot{C}H \rightarrow C_s\bullet + C_2H_2$	$5.0*10^{13}$	159,000
5	$C_sCH\dot{C}H \rightarrow C_s - H + H$	$5.0*10^{10}$	_

Table 5 - Soot reaction mechanism from Colket and Hall with a reaction rate of k = A.exp(-E/(RT))

Using the steady-state approximation for fast reacting intermediates, the mechanism mass growth rate per soot surface is:

$$R_{CH} = \frac{d(mass_growth/m^2)}{dt} = \frac{C_{HACA}(k_1.[H] + k_{-2})(k_4.k_5.[C_2H_2] - k_3.(k_{-4} + k_5))[C_s - H]}{(k_{-1}.[H_2] + k_2.[H] + k_3)(k_{-4} + k_{-5}) + k_4.k_5[C_2H_2]}$$

The coefficient α_{CH} is obtained based on available measurements, after correction for oxidation rates. Correlation between growth rate and R_{CH} is particularly good as can be seen Figure 13. Regression gives α_{CH} = 1.0 with a 95% confidence interval of ±0.2. It confirms that soot growth is well modeled using this mechanism.

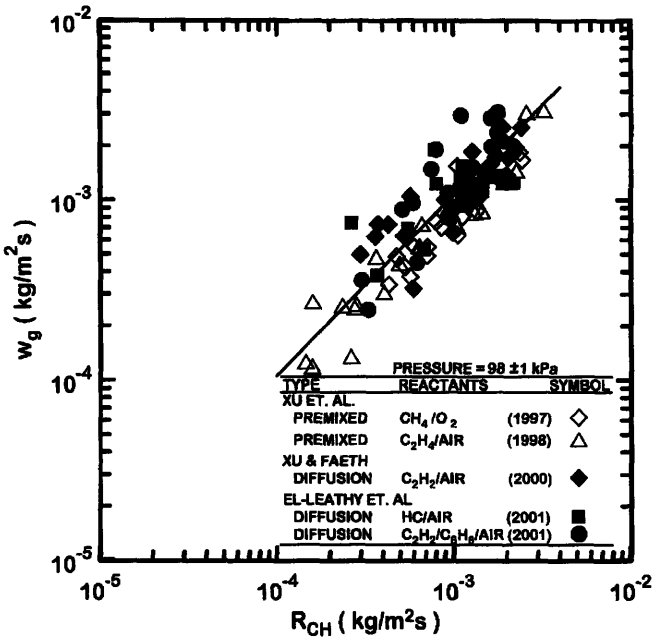


Figure 13 – Soot surface growth rates (corrected for soot surface oxidation) in terms of the HACA mechanism of Colket and Hall for laminar flames at atmospheric pressure (from[31])

The formation rate R_{CH} can be simplified because in usually encountered flame conditions, $[H][C_2H_2]$ varies more than the other terms. It can be approximated as:

$$R_{CH} = cte.{}^{C_{HACA}.k_1.k_4.k_5}\!/_{g(T)}.[H].[C_2H_2]$$

with g being a function of temperature only. Correlation of coefficient α_{CH} depends on the ambient pressure and varies between 0 and 1.

To sum up, the Colket and Hall model for soot creation is:

$$\boxed{w_g = f(T).[H].[C_2H_2]}.$$

[31] AIAA JOURNAL, Vol. 41, No. 5, May 2003, Soot Surface Growth in Laminar Hydrocarbon/Air Diffusion Flames, A. M. El-Leathy, F. Xu, C. H. Kim, and G. M. Faeth

Reaction Mechanism from Kazakov et al.[29]

Kazakov et al. suggested a shorter mechanism to represent soot growth:

Reaction number	Reaction	A (m, kg mol, s)	n	E (kJ/(kg.mol)
1	$C_s - H + H \rightarrow C_s\bullet + H_2$	$2.5*10^{11}$	_	66,900
-1	$C_s\bullet + H_2 \rightarrow C_s - H + H$	$3.9*10^{9}$	_	39,000
2	$C_s\bullet + H \rightarrow C_s - H$	$1.0*10^{11}$	_	_
3	$C_s\bullet + C_2H_2 \rightarrow C_sC_2 - H + H$ (growth)	$8.4*10^{8}$	0.4	35,100

Table 6 - Soot reaction mechanism from Kazakov et al. with a reaction rate of $k = A.T^n.\exp(-E/(RT))$

$C_s - H$ is an armchair site ($[C_s - H] = 2.3.10^{19}$ sites/m^2) and $C_s\bullet$ is a radical site. The soot particle surface growth is $w_g = \alpha_{FW}.R_{FW}$.

Using the steady-state approximation for fast reacting intermediates, the mechanism mass growth rate per soot surface is:

$$R_{FW} = \frac{d(mass_growth/m^2)}{dt} = \frac{C_{HACA}.k_1.k_3.[H].[C_2H_2].[C_s - H]}{k_{-1}.[H_2] + k_2.[H] + k_3.[C_2H_2]}$$

where C_{HACA} is the soot mass per particle and is set to $2M_c/A_v$ (M_c is the carbon molecular weight). α_{FW} is an empirical factor with an order of magnitude of 1, function of the maximum temperature of the flame. R_{FW} is the reaction rate of the mechanism described above.

Data points used to generate the sterical factor for the Colket and Hall mechanism yield a factor of $\alpha_{FW}(T) = 0.0017\exp(12{,}000/T)$.

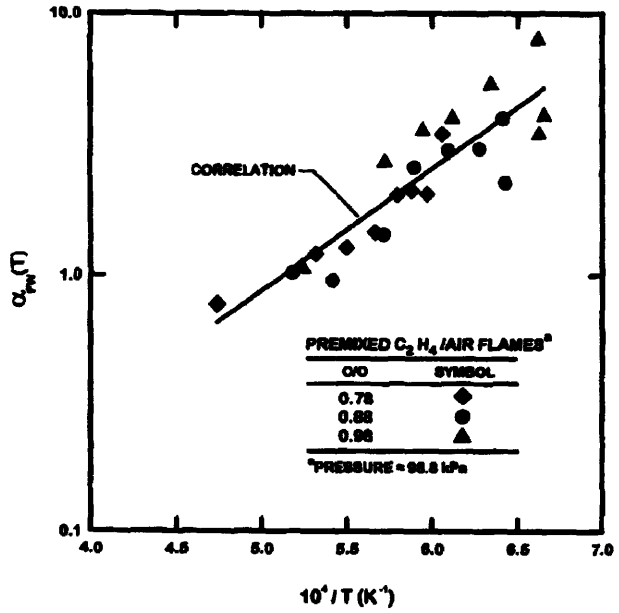


Table 7 - Extrapolation of $\alpha_{FW}(T)$[32]

Just as for R_{CH}, $[H][C_2H_2]$ varies more than the other terms for usually encountered flame conditions. Once again growth rate can be approximated as:

$$\boxed{w_g = f(T).[H].[C_2H_2]}.$$

Estimation of f(T)

Even though correlation for the model has been made using laminar flames only, Z. Wena, S. Yuna, M.J. Thomsona and M.F. Lightstone confirmed the validity of a similar model for turbulent kerosene/air flames[33]. They used the version Lindstedt's model that was developed earlier (see paragraph 3.3.5). The form derived earlier for w_g is assumed to be valid for the combustor model developed in this thesis although no data are available to support this assumption.

The figure below plots $w_g / [C_2H_2]$ as a function of $[H]$. Correlation between both variables is linear with a slope of 1.

---

[32] Combustion and Flame 108:471-493 (1997), Soot Formation in Laminar Premixed Ethylene/Air Flames at Atmospheric Pressure, F. Xu, P. B. Sunderland, and G. M. Faeth

[33] Combustion and Flame 135 (2003) 323–340, Modeling soot formation in turbulent kerosene/air jet diffusion flames

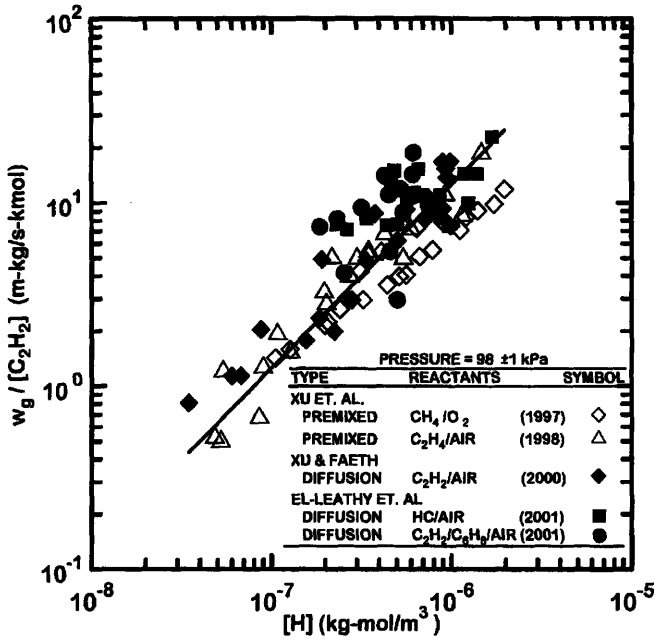


Figure 14 – Estimation of *f(T)*[31]

f(T) is therefore not a function of temperature, and is assumed a constant *c* in the following. The results shown in Figure 14 are not obtained for conditions usually encountered in combustors, i.e. turbulent flames with high pressures, so the extrapolated coefficient *c* might not be valid inside the combustor. For this thesis, the soot growth term $w_g = c.[H].[C_2H_2]$ was used, but the constant *c* was recomputed in order to better match the data.

3.3.3. Oxidation Mechanism

Oxidation of soot can occur from many species. Oxygenated species such as O, H_20, CO_2, OH and O_2 can attack soot,[34] but under most of the conditions, OH and O_2 are the main oxidizing elements.

Modeling of O_2 oxidation

The principal reaction is:

$$C_s + \tfrac{1}{2} O_2 \Rightarrow CO$$

[34] Energy Combust. Sci., Models of Soot Formation and Oxidation, Ian M. Kennedy

The most widely used oxidation model originated from Nagle and Strickland-Constable[35] and considered O_2 as the only oxidizing species (see Appendix D). Another model has been shown to work well in turbulent kerosene and air diffusion flames.[36] This model is based on the work of K. B. Lee et al.[37]. They showed soot oxidation by O_2 can be accurately modeled by the equation:

$$w_{O_2} = -0.1 \cdot 10^5 \cdot [OH] \cdot \sqrt{T} \cdot \exp(-{}^{19,680}/_{T})$$

This function works well when O_2 is in excess like in the cooling areas of the combustor. However, for O_2 concentration below 5% by volume at atmospheric pressure, this function has been shown to underestimate soot oxidation. Under these conditions, O_2, CO_2, H_2O and O are not significant contributors to soot oxidation; OH is the principal oxidant.[38] Both conditions (below and above 5% $[O_2]$ by volume) are present inside the combustor. O_2 oxidation may be dominant near the walls and OH oxidation may be dominant inside the combustor.

Modeling of OH oxidation

The principal reaction is:

$C_s + OH \Rightarrow CO + H$

Estimation of oxidation rates for any species j requires assessment of its collision efficiencies with soot. The collision efficiency η_j of an oxidizing species j is given by:

$$\eta_j = -\frac{4 w_{ox}}{C_j \cdot [j] \cdot \bar{v}_j}$$

where C_j is the mass of carbon removed from the surface for a mole of species j, $[j]$ is the concentration of species j near the soot molecule, and v_j is the mean molecular velocity of

---

[35] Nagle, J., and Strickland-Constable, R.F., "Oxidation of Carbon Between 1000-2000 °C," Proceedings of Fifth Carbon Conference, Vol. 1, 1962, pp. 154-164.

[36] Combustion and Flame 135 (2003) 323-340, Modeling soot formation in turbulent kerosene/air jet diffusion flames, Z. Wen, S. Yun, M.J. Thomson, M.F. Lightstone

[37] K.B. Lee, M.W. Thring, J.M. Beer, Combust. Flame 6 (1962) 137–145.

[38] Combustion and Flame 132 (2003) 43–57, Soot surface oxidation in hydrocarbon/air diffusion flames at atmospheric pressure, F. Xu, A.M. El-Leathy, C.H. Kim, G.M. Faeth

species j, based on Boltzmann equilibrium velocity ($\bar{v}_j = \sqrt{\frac{8.R.T}{\pi.M_j}}$ with M_j the molecular weight of species j). Precision of the method is directly related to the uncertainty of the collision efficiencies. This method works well for OH for instance, as the 95% confidence zone is relatively narrow, but does not achieve good results for O_2. In the O_2 case, uncertainties on collision efficiencies are too high so the first model described above was used for this thesis.

From the definition of collision efficiency for OH:

$$w_{ox} = -\eta_{OH}.\frac{C_{OH}}{4}.[OH].\sqrt{\frac{8.R.T}{\pi.M_{OH}}} = -\eta_{OH}.C_{OH}.\sqrt{\frac{R}{2\pi.M_{OH}}}.[OH].\sqrt{T}$$

Noah et al.[39] studied collision efficiencies for different species. They used predictions of Nagle and Strickland-Constable to estimate attacks from O_2 and measure species collision efficiencies assuming oxidation is due solely to the considered species. They showed the range for collision efficiency is much narrower for OH than for all other potential species – demonstrating that OH is the main oxidant at those conditions – and estimated OH collision efficiency to be 0.14 with a 95% confidence range of ±0.04. This value is in agreement with previous measurements. C_{OH} is equal to 379.

[39] K.G. Neoh, J.B. Howard, A.F. Sarofim, A. F., In: D.C. Siegla, B.W. Smith (Eds.), Particulate carbon. Plenum Press, New York, 1980, p. 261.

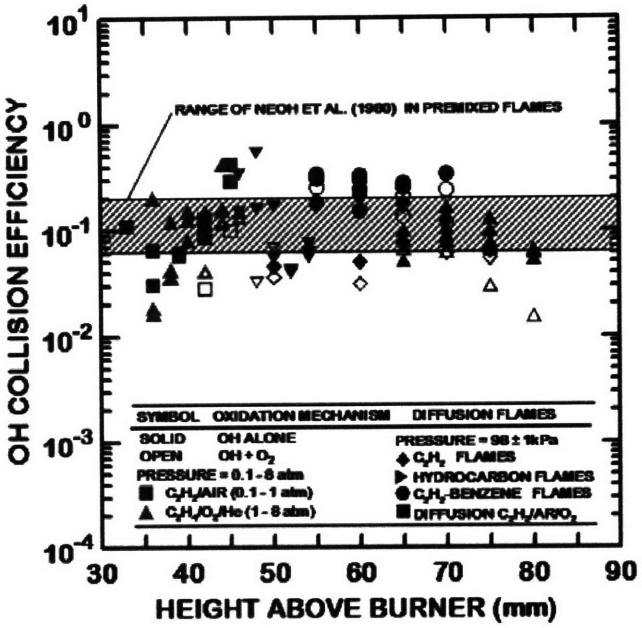


Figure 15 – Collision efficiencies as a function of distance from the burner exit, assuming that soot surface oxidation is only due to attack by OH (from 34).

3.3.4. Coagulation Mechanism

Soot coagulation is modeled using the normal square dependence. The coagulation reaction $nC_S \Rightarrow C_{nS}$ yields a reaction rate q_c equal to:

$$q_c = -2\sqrt{\frac{6k_BT}{\rho_{soot}}}\sqrt{d_p}N^2$$

In this formula, d_P is the soot particle mean diameter and N the particle density.

3.3.5. Lindstedt's Model

Another soot model that has been investigated for implementation in the combustor model is the one suggested by Lindstedt[40]. This model, proposed a few years before the HACA model, does not relate nucleation and soot growth rates to the hydrogen

[40] K.M. Leung, R.P. Lindstedt, Combust. Flame 102 (1995) 129–160.

radical *H*. The equations are basically the same as described previously, except that *[H]* is not present and the constants depend on the ambient temperature. The advantage of using Lindstedt's model is it does not use the radical *H*, so any error modeling *[H]* does not affect soot estimation. Equations for this model are found Table 8 and Table 9.

3.3.6. Modeling Summary

The modeling equations used in this thesis are summarized in the following table. As those values have been obtained for conditions that are not encountered in a combustor, the coefficients are re-computed. It is assumed that the form of the equations is valid under any condition.

Soot mass modeling (in $kg/(m^3.s)$):

Modeling of:	**HACA equations**	**Lindstedt's equations**
Nucleation (w_n)	$c_n \cdot M_P \cdot [C_2H_2] \cdot [H] \cdot e^{5{,}000/T}$	$a \cdot M_P \cdot [C_2H_2] \cdot e^{-21{,}000/T}$
Surface Growth (w_g)	$c \cdot [C_2H_2] \cdot [H] \cdot A_s$	$b \cdot [C_2H_2] \cdot e^{-12{,}100/T} \cdot \sqrt{A_s}$
Surface Oxidation (w_o)	$-c_{OH} \cdot \nu \cdot [OH] \cdot \sqrt{T} \cdot A_s - c_{O_2} \cdot [O_2] \cdot \sqrt{T} \cdot \exp(-19{,}680/T) \cdot A_s$	

Table 8 – Comparison of HACA and Lindstedt's models for mass soot rates

Soot particles modeling (in $part/(m^3.s)$):

Modeling of:	**HACA equations**	**Lindstedt's equations**
Nucleation (q_n)	$c_n \cdot N_A \cdot [C_2H_2] \cdot [H] \cdot e^{5{,}000/T}$	$a \cdot N_A \cdot [C_2H_2] \cdot e^{-21{,}000/T}$
Coagulation (q_c)	$-2 \cdot c_c \cdot \sqrt{\frac{6k_BT}{\rho_{soot}}} \cdot \sqrt{d_p} N^2$	

Table 9 – Comparison of HACA and Lindstedt's models for particle soot rates

In these equations, A_s is the soot surface per volume, d_P is the soot particle mean diameter and a, b, c and all c_i are constant to be fixed later.

A_s and d_P are related to soot mass and soot particle densities as:

$$A_s = (\pi N)^{1/3}\left(\frac{6M}{\rho_{soot}}\right)^{2/3}$$

$$d_P = \left(\frac{6M}{\pi \cdot \rho_{soot} \cdot N}\right)^{1/3}$$

3.4. Discussion of the Physical Parameters Impacting Soot Formation

As can be inferred from Table 9, temperature inside the combustor is one of the most important parameters influencing soot formation. This term is explicitly present in all rates except soot growth, and still, it influences soot growth through species concentration. Other parameters like the chemistry of the fuel, fuel-to-air ratio inside the combustor, and pressure, also play important roles in soot emissions. For instance, chemistry of the fuel plays a crucial role for soot emissions, especially the ratio of hydrogen atoms to carbon atoms[24] (see Figure 8). Fuel-to-air ratio is another major parameter because soot is created in regions where fuel-to-air equivalence ratio is higher than 1.5 [41]. A perfect mixing in a gas turbine combustor would emit no soot as typical overall fuel-to-air ratios in the primary zone of the combustor are around one for high power modes. For this matter, both overall fuel-to-air ratio and mixing are important parameters when considering soot formation. Quality of air and fuel mixing is a difficult parameter to assess. In combustor model used in this thesis, it is modeled with the term s, called the unmixedness parameter, defined as the coefficient of variation for the equivalence ratio distribution of the mass flow into the perfectly stirred reactors (PSRs).

To sum up, temperature, pressure, fuel chemistry, fuel-to-air ratio, and fuel-air mixing are in the most influential parameters for predicting soot emissions.

---

[41] Personal communication with Meredith B Colket, at UTRC

Assessment of soot emission at other altitudes and other modes

The parameters previously mentioned can be used to assess emissions at other operating conditions than standard measurements. For instance, if we know emissions at sea level for a power setting for a specific engine and we want to assess emissions at the same power but for different conditions, we need a relation between emissions on the one hand and temperature, pressure and fuel-to-air ratio on the other hand. In this case, fuel chemistry does not change between both conditions, and fuel-air mixing is considered the same. Döpelheuer interpolated these functions and showed that for any combustor, the soot emission index at cruise can be estimated from the soot emission index at sea level by using the following formula[42]:

$$C_{soot} = C_{soot,ref} \cdot \left(\frac{\phi}{\phi_{ref}}\right)^{2.5} \cdot \left(\frac{P_3}{P_{3,ref}}\right)^{1.35} \cdot \frac{e^{(-20{,}000/T_f)}}{e^{(-20{,}000/T_{f,ref})}}$$

where C is the soot concentration (equivalent to CI in the FOA method), ϕ is the fuel-to-air equivalence ratio, P_3 is the pressure at the exhaust of the compressor and T_f the flame temperature inside the combustor. This relation shows the importance of determining the important variables in our analysis.

[42] "Quantities, Characteristics and Reduction Potentials of Aircraft Engine Emissions", Andreas Döpelheuer, Society of Automotive Engineers, Inc., 2001

Chapter 4

Insertion of the Soot Model

This chapter illustrates how the soot equations described previously are integrated in the existing reactor network combustor model. We first detail more thoroughly how the combustor model works and then compute the equations that will be used in the MATLAB® code to generate soot exhaust flows.

4.1. The Combustor Model

The combustor model developed by Allaire[7] has 5 input variables (T_3, P_3, volume of combustor, $\dot{m}_{air}$, $\dot{m}_{fuel}$ and s, representative of how well-mixed the air and fuel are) that are used to compute emission indices for the different compounds. $\dot{m}_{air}$ and $\dot{m}_{fuel}$ are the total airflow and fuel flow entering the combustor. The combustor is divided into 4 sequential zones that are the primary zone (PZ), the intermediate zone (IZ), the dilution zone (DZ) and the remaining zone (RZ) as shown in Figure 16. Air from the dilution holes (blue arrows) is mixed with gases at the beginning of each zone modeling the dilution air that is injected inside a combustor. An optimizing code is run to determine how much air goes through the arrows and how much air goes inside the primary zone. T_3 and P_3 set the operating temperature and pressure when air and fuel are inserted into the primary zone.

The purpose of the optimizing code is to set "internal" parameters with the objective of minimizing a function f based on the difference between the emissions from the model and ICAO data. These "internal" parameters are:

- Fractions of the combustor volume that are associated with the primary zone, the intermediate zone, the dilution zone and the remaining zone.
- Fractions of the combustor inlet air flow that enter each of those zones.

- Unmixedness of the 4 ICAO points.

The objective function f computes the difference between emissions from the model and ICAO data.

$$f = \sum_{i=1}^{4} f_i$$

where the subscript i refers to the ICAO LTO cycle point (idle, approach, climb-out and take-off) and where:

$$f_i = \left(\frac{Model_EINO_{xi} - ICAO_EINO_{xi}}{\sum_{i=1}^{4} ICAO_EINO_{xi}} \right)^2 + \left(\frac{Model_EICO_i - ICAO_EICO_i}{\sum_{i=1}^{4} ICAO_EICO_i} \right)^2$$

When soot emissions are included in the model, the function is modified to take into account soot emissions. The term $\left(\frac{Model_EIsoot_i - ICAO_EIsoot_i}{\sum_{i=1}^{4} ICAO_EIsoot_i} \right)^2$ is added to the functions f_i..

The equivalence ratio in the primary zone is defined as $\phi_{PZ} = \frac{\dot{m}_{fuel}}{0.0641 \cdot \dot{m}_{air_PZ}}$, $\dot{m}_{air_PZ}$ being the total airflow going inside the primary zone. 16 parallel Perfectly Stirred Reactors (PSRs) are used to model the primary zone and the different mixing of air and fuel in this area. Each PSR has a different fuel-to-air ratio that goes from 0 to $2\phi_{PZ}$. The importance of each PSR, i.e. how much of the total flow (air + fuel) in the primary zone goes inside each PSR, is modeled using a normal distribution with mean ϕ_{PZ} and variance $s\phi_{PZ}$, with the tails cut out below 0 and over $2\phi_{PZ}$. The distribution is then re-normalized. This distribution is representative of the different fuel-to-air concentration areas inside the combustor and representative of the space they use, where ignition of the mixture occurs.

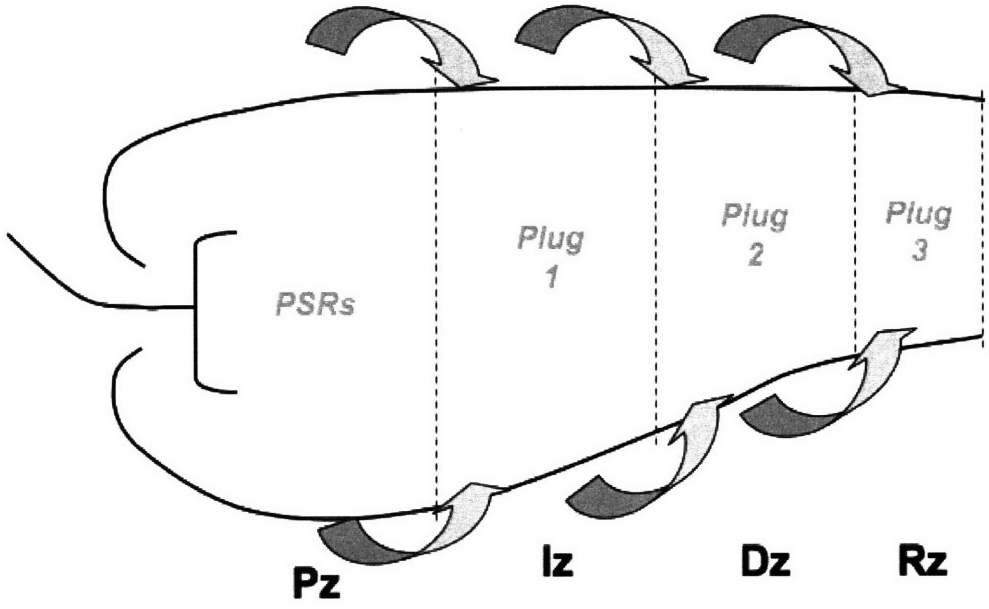


Figure 16 – Different areas inside the combustor

After the primary zone, gases from all PSRs are collected and mixed together, then mixed with air. The mixture goes through plug #1, a one-dimension reactor representative of the intermediate zone of the combustor. Downstream of the plug, air is mixed with the resulting mixture, gases go through plug #2, then air is added and finally the mixture goes through plug #3. Gases at the combustor exit are gases at the exit of plug #3. Emission indices are determined at this stage by division of the considered species mass flow by the total fuel flow.

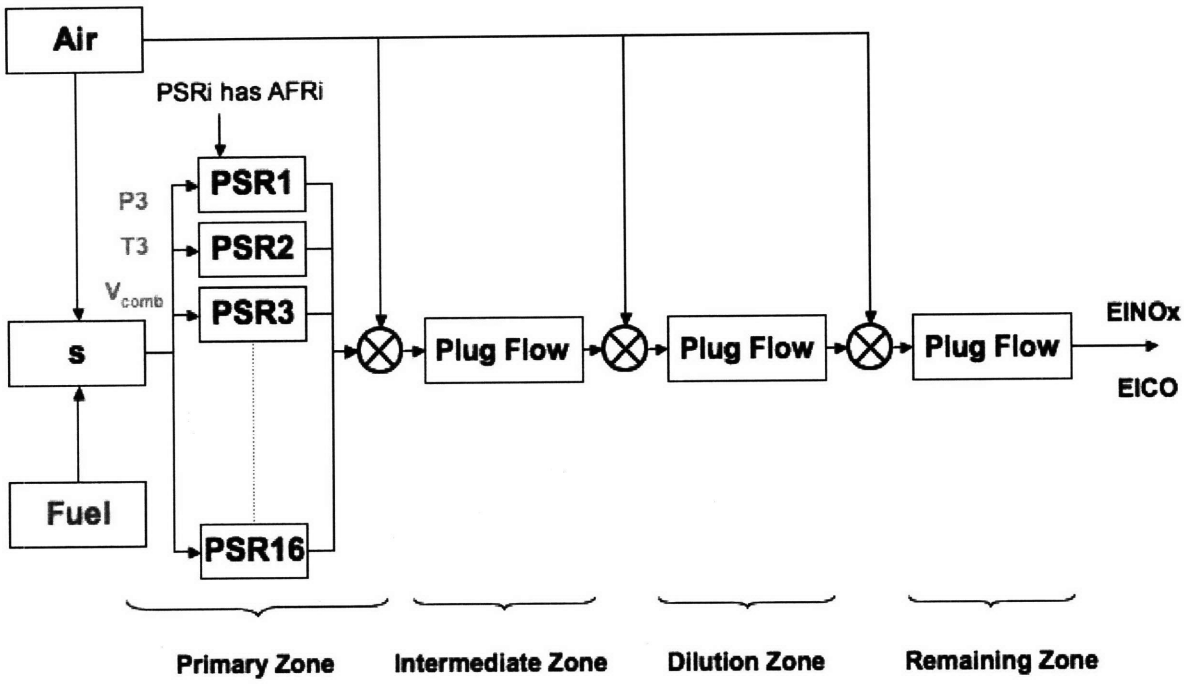


Figure 17 – Functional outline of the combustor model

4.2. Computation of Soot Emissions in PSRs and PLUGs

The overall objective of the combustor model is to determine soot mass and particle flows at the combustor exit. Local equations for soot creation and soot oxidation have been set up as described in paragraph 3.3.6, and need to be integrated in order to get soot mass and soot particle flows. Assuming one has knowledge of soot mass density (noted M and in kg/m^3) and to soot particle density (noted N and in $part/m^3$) at any time and any position in the combustor, then it is necessary to compute combustor exhaust soot flows.

Let us consider a volume _ (either a PSR or a PLUG) at steady state and note $A(x)$ the cross-section area perpendicular to the flow (see Figure 18) at a distance x downstream of the inlet. Time τ is required for the gases to go through volume _. Let $\dot{m}_s(x)$ and $\dot{n}_s(x)$ respectively be the soot mass flow and the soot particle flow through this cross-section and $\dot{m}_s$ and $\dot{n}_s$ their values at the exit of the volume.

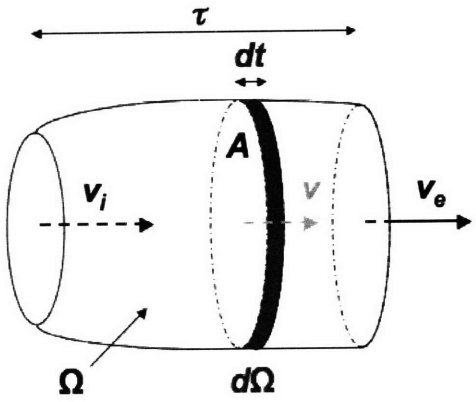


Figure 18 – Volume _

4.2.1. Soot Modeling Integral Equations

We consider the volume $d_ = A(x).dx$ between x and $x + dx$, and we want to determine $\dot{m}_{s_out} - \dot{m}_{s-in} = d\dot{m}_s$, the difference between the outlet and inlet soot mass flow at steady state. This difference is equal to the variation of soot mass in $d_$, so that

$$d\dot{m}_s = \frac{d}{dt}(M.d\Omega) = \frac{d}{dt}(dm_s) \qquad (5)$$

with dm_s the total mass of soot in volume $d_$.

The variation of dm_s is non-zero in cases where soot is created or consumed. We defined w_m as the sum of the nucleation, the growth, and the oxidation mass soot rates per soot area ($w_m = w_n + w_g + w_o$ and is expressed in $\frac{kg}{s}.\frac{1}{m^2}$). w_m can be expressed as a function of the variables ρ, ρ_s, f_s and A_s (respectively, the density of the fluid, soot density of a soot particle, volume fraction of soot, and soot surface per volume):

$$w_m(M,N) = \frac{\rho}{A_s}\frac{d}{dt}(\rho_s.f_s/\rho) = \frac{\rho}{A_s}\frac{d}{dt}(\frac{dm_s}{dV_s}.\frac{dV_s}{d\Omega}.\frac{d\Omega}{dm}) = \frac{1}{A_s.d\Omega}\frac{d}{dt}(dm_s) \qquad (6)$$

dV_s being the volume occupied by soot, A_s the soot area per volume, and dm the total mass of volume $d_$.

Thus, the local relation is $d\dot{m}_s = A_s.d\Omega.w_m$. Integration of this relation over a cross section leads to:

$$\boxed{\frac{d\dot{m}_s}{dx} = w_m.A_s.A(x)} \qquad (7)$$

By integration, we obtain:

$$\boxed{\dot{m}_{s_exit} - \dot{m}_{s_inlet} = \int_0^l A_s.w_m.A(x).dx} \qquad (8)$$

We apply the same procedure for particle density.

$$d\dot{n}_s = \dot{n}_{s_outlet} - \dot{n}_{s_inlet} = \frac{d}{dt}(N.d\Omega) = \frac{d}{dt}(dn_s)$$

Soot particle evolution is modeled through the term w_n, the sum of the nucleation and coagulation soot rates (expressed in *part/s*).

$$w_n = \rho\frac{d}{dt}(N/\rho) = \rho\frac{d}{dt}(\frac{dn_s}{d\Omega}.\frac{d\Omega}{dm}) = \frac{1}{d\Omega}\frac{d}{dt}(dn_s)$$

with dn_s as the total number of soot particles in volume $d_$.

Integration of this relation over a cross section leads to:

$$\boxed{\frac{d\dot{n}_s}{dx} = w_n(x).A(x)} \qquad (9)$$

By integration, we obtain:

$$\boxed{\dot{n}_{s_exit} - \dot{n}_{s_inlet} = \int_0^l w_n.A(x).dx} \qquad (10)$$

Given geometry, a relationship between mass and particle soot flows on the one hand, and mass and particle soot densities on the other hand is required to solve equations 8 and 10.

4.2.2. Relation between Soot Flows and Soot Densities

Let us consider a cross section $A(x)$ at a distance x downstream of the inlet. For a time dt that is infinitely small, a mass $\dot{m}_s(x).dt$ of particles cross section $A(x)$. The particles crossing are the ones located less than a distance $v(x).dt$ upstream of the section, with $v(x)$ the average gas velocity on the considered cross section. We obtain the relation $\dot{m}_s(x).dt = M(x).A(x).v(x).dt$.

The particle flow equation for soot particles is:

$$\dot{m}_s(x) = A(x).v(x).M(x) \quad \forall x \qquad (11)$$

Doing the same analysis for particle flow, we get the relation:

$$\dot{n}_s(x) = A(x).v(x).N(x) \quad \forall x \qquad (12)$$

Typical velocities inside the combustor are around Mach number $M = 0.25$, so that $M^2 \approx 0.063$. We consider M^2 is small enough for the flow to be considered incompressible, so that flow across any section is constant. It results in $A(x).v(x)$ being constant and equal to $A.v$ along the x axis, and integration of $d\Omega = A.v.dt$ from 0 to τ leads to $A.v.\tau = \Omega$.

Thus,
$$\boxed{A.v = \Omega/\tau} \qquad (13)$$

and
$$d\Omega = dt.\Omega/\tau \qquad (14).$$

From the relations above, we derive the relationship between soot flows and soot densities:

$$\dot{m}_s(x) = \Omega/\tau.M(x) \quad \forall x \qquad (15)$$

$$\dot{n}_s(x) = \Omega/\tau.N(x) \quad \forall x \qquad (16)$$

4.2.3. Soot Equations System

Equation 11 leads to $A.dx = dt.\Omega/\tau$. We insert it in equations 7 and 9 and obtain:

$$\boxed{\frac{d\dot{m}_s}{dt} = A_s(M,N).w_m(M,N).\Omega/\tau} \qquad (17)$$

Doing the same for particle density leads to:

$$\boxed{\frac{d\dot{n}_s}{dt} = w_n(M,N).\Omega/\tau} \qquad (18)$$

Note that w_g and w_n are both functions of M and N, so we can group equations 17 and 18 as a system of equations – 4 equations with 4 unknowns – that we can solve. $\dot{m}_s$ and $\dot{n}_s$, and the mass flow and particle flow at the exit of each volume, are obtained solving the following system:

$$\begin{cases} \dfrac{d\dot{m}_s}{dt} = \dfrac{\Omega}{\tau}.A_s(M,N).w_g(M,N) \\ \dfrac{d\dot{n}_s}{dt} = \dfrac{\Omega}{\tau}.w_g(M,N) \\ \dot{m}_s = M.\dfrac{\Omega}{\tau} \\ \dot{n}_s = N.\dfrac{\Omega}{\tau} \\ \dot{m}_s(0) = \dot{m}_{s_initial} \\ \dot{n}_s(0) = \dot{n}_{s_initial} \end{cases}$$

4.3. Chemical Kinetics Models

The model uses software *Chemkin*® to compute species concentrations in PSRs and PLUGs throughout the combustor model. The chemical model inserted in the combustor model is the GRI-Mech combustion model developed in partnership between the University of California, Berkeley, Stanford University, SRI International and the University of Texas at Austin[43]. GRI-Mech is an optimized detailed chemical reaction mechanism capable of representing natural gas flames and ignition. It is one of the most utilized chemical kinetics models for natural gas combustion and predicts accurately composition of natural gas flames. The model uses 53 species, listed in appendix C. Its inherent simplicity – due to the few species used – is both a strength and a weakness. The strength is it can model accurately reactions in flames and still keep computation time low. The weakness is there are only 2 hydrocarbons with more than 2 atoms of carbon (C_3H_7 and C_3H_8) so there is no aromatic in the model. This was not a problem for modeling NO_x and CO emissions but can lead to poor estimates of soot growth and soot nucleation modeling.

In order to offset the aromatics problem, another chemical kinetics mechanism has been tested. Dr. Lourdes Maurice developed a model on the basis of the GRI-Mech model, with a purpose to more adequately model jet fuel[44]. With the idea of modeling more details relevant to jet fuel combustion, she added an aromatics scheme. A total of 179 species are listed in this model (see Appendix D). The strengths and weaknesses of such a model are opposite of the GRI-Mech model. It should indeed capture the creation of soot and acetylene, but will take a longer time to run.

Both models have been tested in this thesis to determine which one should be used in the combustor model and results are indicated in the following chapter.

---

[43] Gregory P. Smith, DavidM. Golden, Michael Frenklach, NigelW. Moriarty, Boris Eiteneer, Mikhail Goldenberg, C. Thomas Bowman, Ronald K. Hanson, SoonhoSong, William C. Gardiner, Jr., Vitali V. Lissianski, and Zhiwei Qin, "GRI mech 3.0," http://www.me.berkeley.edu/gri-mech/.

[44] Maurice, L. Q., "Detailed Chemical Kinetic Models for Aviation Fuels," Ph.D. Thesis, Univ. of London, London, Oct. 1996.

Chapter 5

Results Discussion

As engine data are proprietary, there is little public information available on the evolution of soot inside recent combustors. As a result, it is difficult to know precisely how soot behaves inside the combustor. We know that soot is created, grows and then gets oxidized, but the question of the presence of a soot concentration peak, as well as the location and the intensity of such a peak, are important questions that cannot be answered precisely. Answers to these questions would allow us to set up the soot equation coefficients and would greatly enhance the precision of our model. Because we do not have access to these data, it is important to understand that the study is based on getting reasonable soot values from the model. In this chapter, we detail what choices were made for the soot model and analyze the sensitivity of the model.

5.1. Selection of the Soot Model

As discussed above, different fuel types, different soot models or different kinetics models can be used to model soot emissions. The purpose of this section is to describe the assessments that were made to select the best combination of these alternatives. The assessment was performed using a PW4090 engine model.

5.1.1. Selection of the Kinetics Model

As described in the previous chapter, two kinetic models were used in Chemkin. The first implementation of soot equations – based on Lindstedt's model – showed very low levels of soot formation in the primary zone, resulting in low overall soot emissions from the combustor. Therefore both kinetics models were implemented and the effects on

C_2H_2 concentrations were analyzed (since C_2H_2 is the primary species responsible for soot formation). For this test, the soot formation model is Lindstedt's.

As seen Figure 19, C_2H_2 molar fractions increase slightly with the most detailed model. However, the change is little and leads to computations problems. Indeed, the more detailed model had trouble converging for short residence times, as well as for too high equivalence ratios. Computation times with the complex model also increase by as much as ten times relative to the simple model.

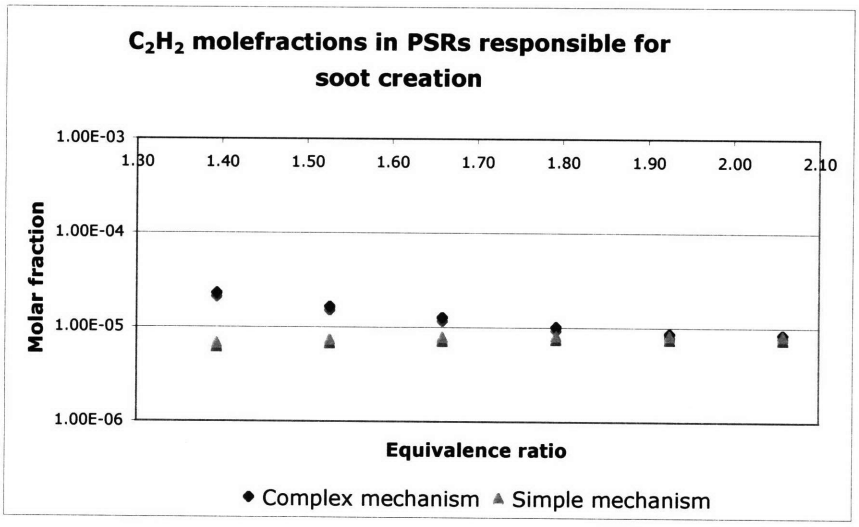


Figure 19 – C_2H_2 differences for the simple and the complex kinetics mechanism. Residence times are obtained for TO conditions. Molar fractions are representative of other modes as well.

Even though improvements of acetylene concentrations for the complex kinetics model are interesting, its implementation caused too many convergence problems and increased computation times too much to be useful for the purposes of this study. The simple kinetics model was therefore chosen for use for the work presented in this thesis.

5.1.2. Choice of the Soot Formation Model

Two soot formation models are compared in this section: the HACA mechanism and Linstedt's model. Both models use the simple kinetics mechanism. For PSRs with equivalence ratios in the range [0,3], soot formation at the exhaust was estimated at takeoff and climb-out powers. Results are shown Figure 20. Soot concentration at

takeoff and climb-out are very similar (when considering a PSR with a fixed equivalence ratio, the change in power affects only the residence time, so it is not surprising that these two plots are similar at takeoff and at climb-out). These plots are a function of residence times only.

Based on the concentration index found in the FOA 3.0 method (page 30), the soot concentration in the turbine exhaust associated with a Smoke Number of 7.2 – the ICAO value for the PW4090 engine at takeoff – is 0.79 mg/m^3. We expect soot concentrations at the end of the primary zone to be at least one or two orders of magnitude above 0.79 mg/m^3. As shown in Figure 20, the maximum soot concentration for the Lindstedt model is less than 1 mg/m^3 at takeoff and at climb-out. On the other hand, the HACA model has concentration peaks above 10 mg/m^3 and almost reaches 100 mg/m^3 for both powers. This pattern was confirmed with the CFM56-2C model. Lindstedt's model underestimates soot formation therefore the HACA model was selected for further use.

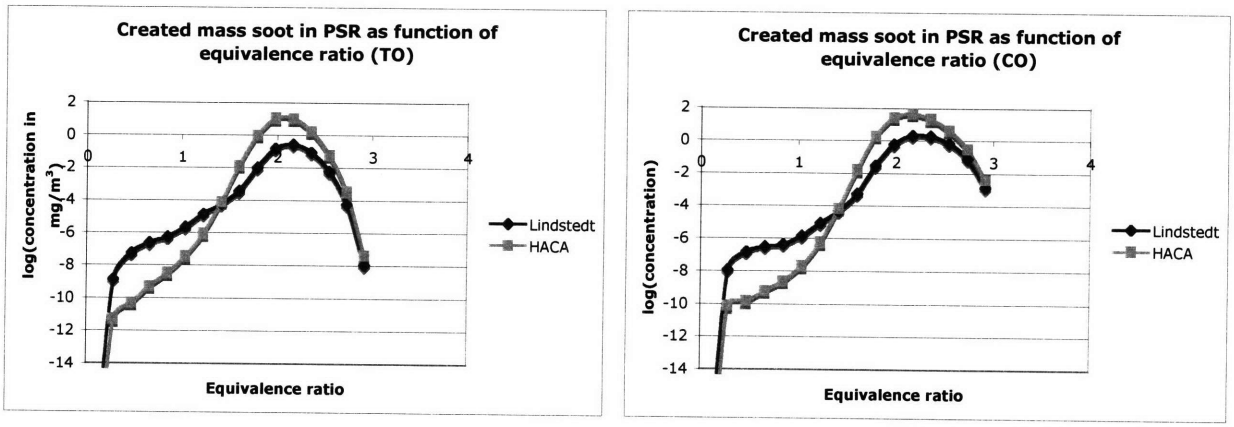


Figure 20 - Formation of soot in PSRs for both soot models

It is interesting to note that soot formation shapes look similar for both models. The models confirm that there is no soot formed below equivalence ratios of about 1.5 (see page 58). Finally, for too high equivalence ratios, soot formation is low as the mix of air and fuel is too rich to burn well and to form acetylene and hydrogen. These features give confidence in the model.

5.1.3. Selection of the Unmixedness Representation

Below are compared two unmixedness distributions. We explain the reasons of the switch to a beta distribution and show the improvement achieved.

Truncated Normal Distribution

The combustor model previously developed uses a selection of 16 PSRs to model the primary zone, each of which has a different equivalence ratio. For each operating mode (idle, approach, climb-out or takeoff), a choice is made to cover a range [*0 ;* ϕ_{mode_max}] of equivalence ratios. Each PSR is labeled – numbered i – and has an equivalence ratio ϕ_i equal to $\phi_i = \frac{1+2\cdot(i-1)}{32}\phi_{mode_max}$.

In the previous model, the fraction $f(PSR_i)$ of air that enters PSR i, relative to the overall air entering the primary zone, is determined using a cumulative normal distribution. For symmetry reasons, ϕ_{mode_max} is taken equal to $2*\phi_{PZ}$, where ϕ_{PZ} is the mean equivalence ratio in the primary zone model. Because the difference between 2 equivalence ratios is $\phi_{mode_max}/16$, the fraction $f(PSR_i)$ of air that enters PSR i is equal to:

$$f(PSR_i) = \frac{CDF(\phi_i + \phi_{mode_max}/32) - CDF(\phi_i - \phi_{mode_max}/32)}{CDF(\phi_{mode_max}) - CDF(0)}.$$

with CDF the cumulative normal distribution.

Figure 21 shows $f(PSR_i)$ values for an unmixedness value of $s = 0.4$ and a mean equivalence ratio of $\phi_{model_PZ}=1$.

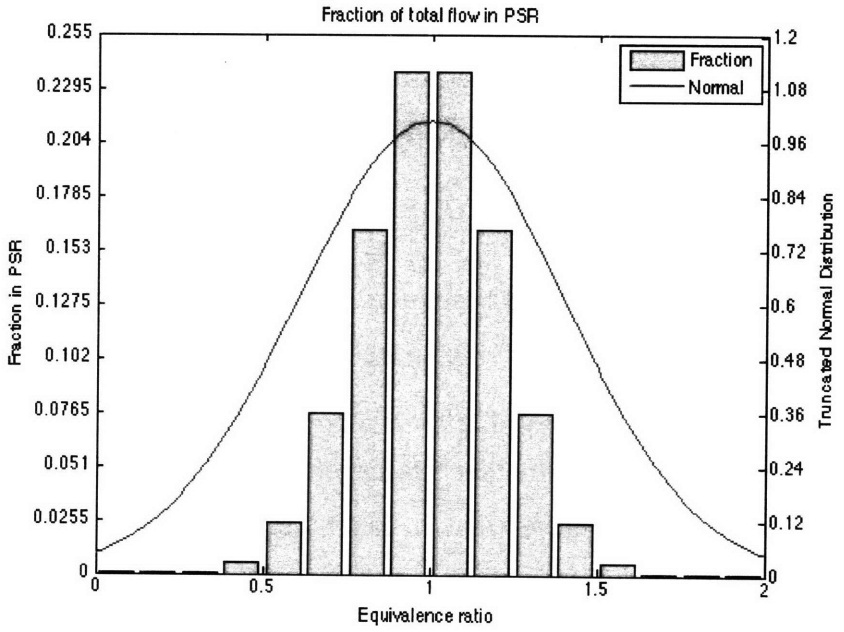


Figure 21 - Fraction of flow going into PSRs for a truncated normal distribution. Note the importance of the PSRs with equivalence ratios close to the mean and the very low importance of low and high equivalence ratios

Further investigation has shown that the truncated normal distribution cannot model adequately soot formation for all engine powers. The reason is that the maximum equivalence ratio is equal to $2*\phi_{PZ}$, so for low ϕ_{PZ} values, no PSR has an equivalence ratio high enough – i.e. above 1.5 – to form soot. For instance, idle and approach powers have too low mean equivalence ratios to model soot creation in the model, even though soot emissions exist at those powers. Other limitations of the truncated normal distribution are that most of the flow is concentrated in areas with fuel-to-air ratios close to the mean, so fuel and air are almost perfectly stirred in the primary zone. This is not true for all combustors, especially the oldest ones that did not achieved excellent mixing, so the model does not capture different technologies of combustors. The reality is that there are large regions in the combustors' primary zone that have no fuel. This cannot be modeled by a normal distribution as those regions have extremely low importance in the truncated normal distribution.

The new distribution needs to have a wider equivalence ratio range, it must give more importance to low equivalence ratios, and must model different combustor technologies. It must model combustors that achieve poor mixing, good mixing, and in between.

Beta Distribution

The distribution selected is a beta distribution. The main advantage of this group of functions is they do not have to be symmetrical. For this matter, the length of the segment is not restricted to $2\phi_{model_PZ}$ and we can increase the equivalence ratio distribution length to model soot. Another interest of the beta distribution, compared to the truncated normal distribution, is that it can more properly model areas of the combustor in which there is only air. The probability of having low equivalence ratios can indeed be high when using a beta distribution, whereas it has to stay low with a truncated normal distribution. A beta distribution is a more flexible, and therefore potentially more accurate representation of what occurs in combustors.

Definition of beta distributions

Beta distributions are a family of continuous probability distributions that are defined on the interval *[0,1]*. They use two parameters α and β that define the shape of the distribution. The probability density function *f* of any of these distributions is written as:

$$f(x;\alpha,\beta) = \frac{x^{\alpha-1}\cdot(1-x)^{\beta-1}}{\int_0^1 u^{\alpha-1}\cdot(1-u)^{\beta-1}du} \text{ for } \begin{cases} x \in [0,1] \\ (\alpha,\beta) \in (IR^+)^2 \end{cases}.$$

The mean of the distribution is $\mu = \frac{\alpha}{\alpha+\beta}$ and the variance $\sigma^2 = \frac{\alpha\beta}{(\alpha+\beta)^2(\alpha+\beta+1)}$.

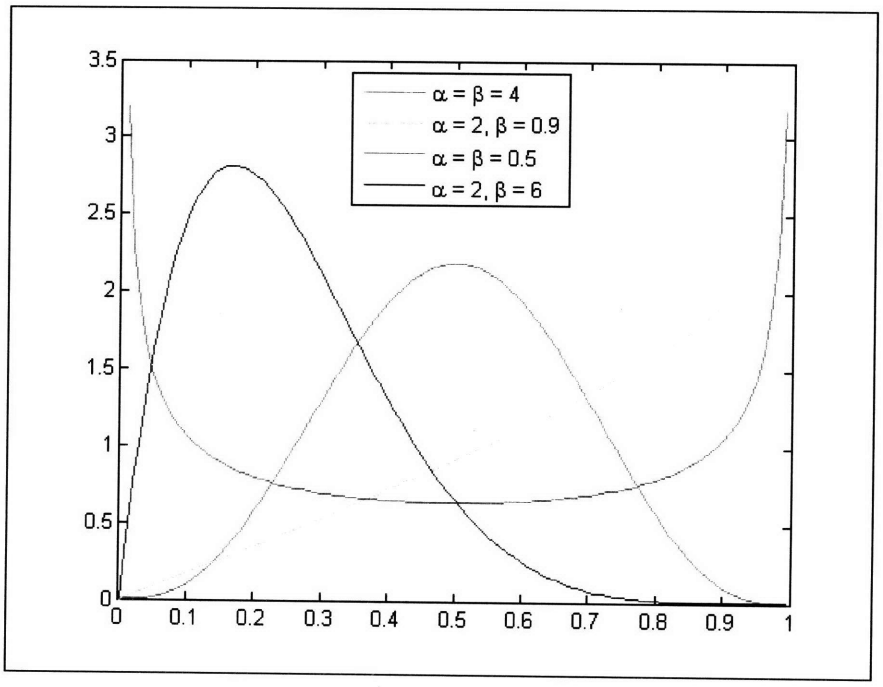


Figure 22 – Beta distributions for different values of α and β obtained with MATLAB®

When we scale up the distribution to the definition domain $[0,\delta]$, the mean and variance of the distribution are $\mu = \delta \cdot \frac{\alpha}{\alpha+\beta}$ and $\sigma^2 = \delta^2 \cdot \frac{\alpha\beta}{(\alpha+\beta)^2(\alpha+\beta+1)}$, and the distribution function is:

$$f(x;\alpha,\beta) = \frac{1}{\delta}\frac{\left(x/\delta\right)^{\alpha-1}\cdot(1-x/\delta)^{\beta-1}}{\int_0^1 u^{\alpha-1}\cdot(1-u)^{\beta-1}du} \text{ for } \begin{cases} x \in [0,\delta] \\ (\alpha,\beta) \in IR^2 \end{cases}.$$

Mean equivalence ratio and standard deviation (s*ϕ) are known in the model and are used to compute coefficients α and β, using the following relations:

$$\begin{cases} \alpha = \frac{\mu}{\delta}\cdot\left(\frac{\mu^2}{\sigma^2}-1\right) = \frac{\mu}{\delta}\cdot\left(\frac{1}{s^2}-1\right) \\ \beta = \left(1-\frac{\mu}{\delta}\right)\cdot\left(\frac{\mu^2}{\sigma^2}-1\right) = \left(1-\frac{\mu}{\delta}\right)\cdot\left(\frac{1}{s^2}-1\right) \end{cases}$$

α and β are two positive coefficients in order for the integral of f to be finite. Because $\mu < \delta$, the required condition is that $\mu > \sigma$, or $\underline{s < 1}$.

Tests were performed using a HACA model for soot formation and the simple kinetics model. We fix the maximum equivalence ratio to 2 for the beta distribution (maximum value for the truncated normal distribution in this case). All model parameters are held constant for the two models. Computations show the improvement and stability of soot creation for the beta distribution model as shown in Figure 23. Takeoff values are similar for both distributions because maximum equivalence ratios are similar (see Table 10). The difference is visible for low powers. There are at least 3 orders of magnitude difference between the distributions. For the normal distributions, no soot is present in the exhaust for both engines. For beta distributions, soot formation is more stable, and for this reason, this type of distribution is chosen to model the PSR relative importance. We must note that higher maximum values can be chosen for beta distributions, this will make the difference with normal distributions even larger.

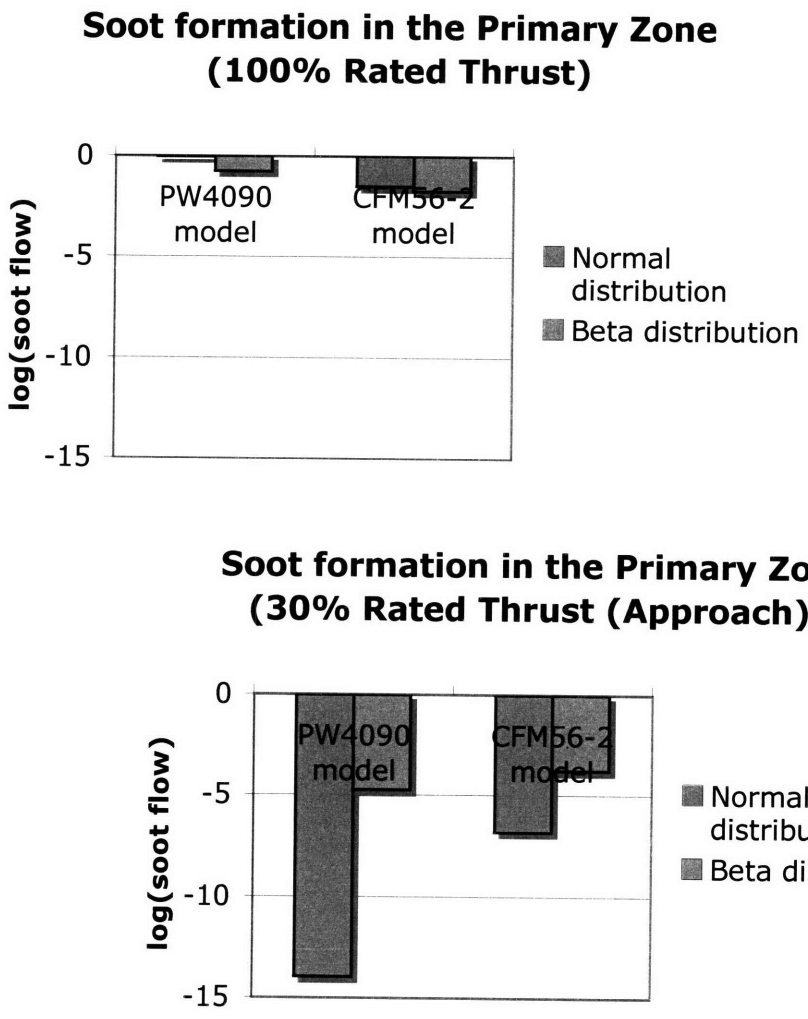


Figure 23 – Formation of soot in the primary zone for TO and AP powers. Note that soot emissions for takeoff and approach are more stable for the beta distribution than for the normal distribution

The switch to beta distributions increases greatly combustor soot formation estimates because the maximum equivalence ratio is higher. Maximum equivalence ratios are shown Table 10. We can see that the bigger the difference is for the maximum equivalence ratio, the bigger the difference is for soot formation.

	Normal distribution PW4090 model	Normal distribution CFM56-2 model	Beta distribution (both engines)
Idle	0.62	1.41	2
Approach	1.18	1.72	
Climb-out	1.86	1.95	
Takeoff	2.06	1.92	

Table 10 – PW4090 and CFM56-2 models: maximum equivalence ratios for the 4 ICAO points

Final distributions obtained for the PW4090 at different ICAO modes are shown below.

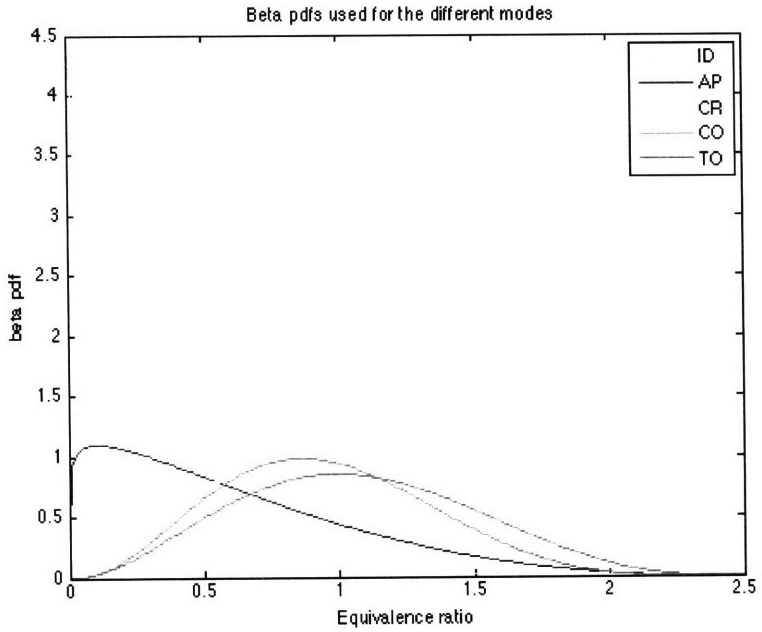


Figure 24 – PW4090: Beta pdf used to model ICAO modes emissions. Note that the maximum equivalence ratio has been increased to 2.5 in order to more accurately represent soot emissions.

5.1.4. Choice of the Fuel Model and Aromatics Representation

The chosen chemical kinetics model – the GRI model – has been developed for propane fuel and has shown satisfying results for NO_x and CO emissions. The goal is to have similar models for NO_x, CO and soot, so we decided to keep this model and to keep propane as a fuel surrogate. However, the hydrogen content is higher for propane than for kerosene since hydrogen mass percent is 18.2% for propane and 15.3% for kerosene

(taking an approximate chemical composition[24] of $C_{12}H_{26}$). This should lead the model to underestimate soot emissions by as much as 40% (see Figure 8) and we need to compensate for this reduction in emissions level. One of the reasons why hydrogen content is high is that there are no complex hydrocarbons, nor aromatics modeled in the propane fuel. In order to decrease the hydrogen content, but also to boost soot formation, we include a species that results of the presence of aromatics: acetylene. Acetylene has indeed a hydrogen mass percent of 7.7% and is formed through aromatics. Another interesting aspect of increasing acetylene content in the fuel is to bypass the formation of acetylene created through PAHs, as those species are not modeled by the mechanism.

We studied the influence of increasing the aromatics content in the fuel through the addition of acetylene (Figure 25). The study was conducted using a HACA mechanism for the soot formation, a beta pdf, and the simple kinetics model.

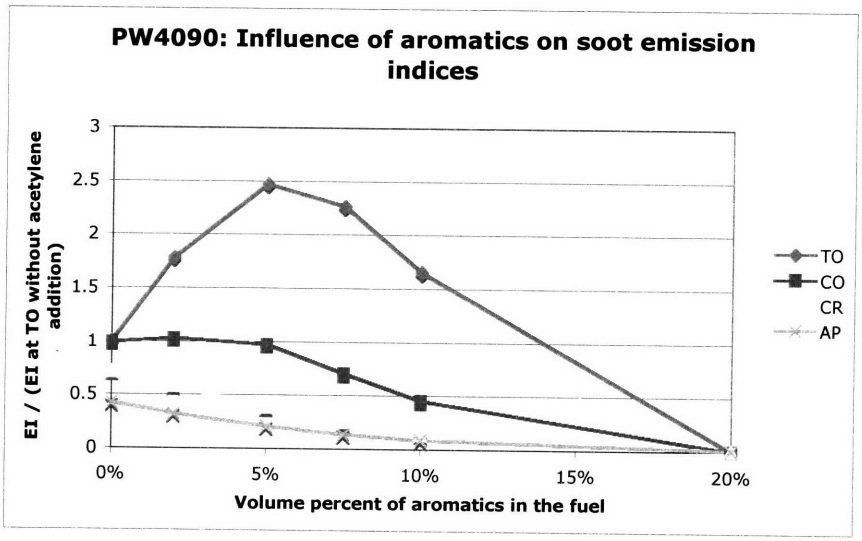


Figure 25 – Influence of addition of acetylene on soot EI. Y-axis is normalized by the engine maximum EI obtained without acetylene addition.

Small additions of acetylene increase soot emissions and can make up for the decrease in soot emissions due to the model higher hydrogen content. However, further analyses showed the increase was produced in an unrealistic way. Indeed, as Figure 26 shows, the increase in emissions is obtained by increasing C_2H_2 molar fractions for low equivalence ratios (to the contrary of high powers whose molar fractions stay constant with or without acetylene addition). The reason why low equivalence ratios have higher

C_2H_2 molar fractions is because the equivalence ratio is too low for reactions to occur, so molar fractions in these PSRs do not evolve between the inlet and the outlet. Molar fraction of acetylene increases with fuel-to-air equivalence ratio – the increase is actually linear – because 10% of the fuel is acetylene and no reaction occurs. Because the soot change is not physics-based, we do not include acetylene in the fuel.

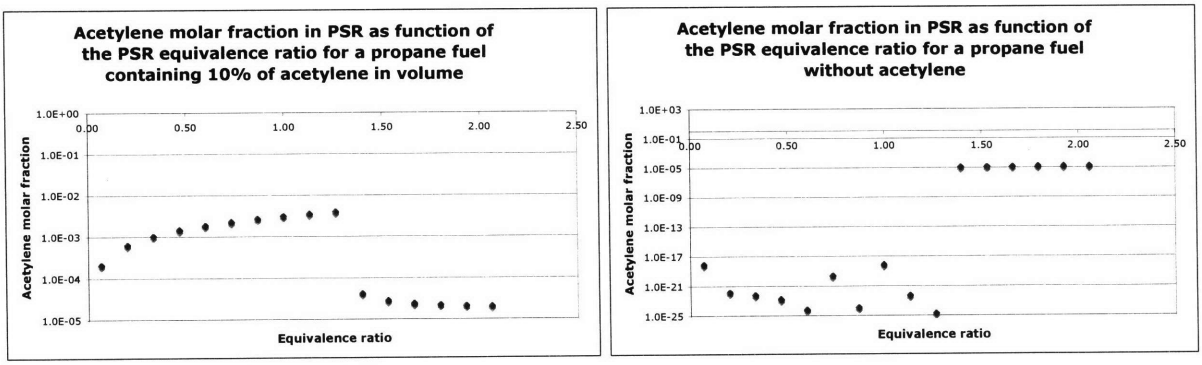


Figure 26 – Comparison of acetylene molar fraction as function of equivalence ratios for a propane fuel containing 10% of acetylene in volume and propane fuel containing no acetylene. Note that logarithmic scales are different for the plots.

To sum up, the chosen model is the HACA mechanism for soot formation, the simple kinetics mechanism for the chemistry, no aromatics modeled in the fuel and a beta distribution for unmixedness inside the primary zone.

5.2. Correction of the Model

However, once all "internal" parameters were set to minimize the objective function described page 61 (updated for soot), the soot mechanism did not prove to correctly estimate soot emissions, and did not model the right trend of emissions. In addition, it appeared extremely sensitive to inputs.

The main problem is, for high powers, NO_x and soot evolve in different ways with the unmixedness parameter (s). As s increases, NO_x model emissions decrease and soot model emissions increase as shown in Figure 27 and Figure 28. Because NO_x emissions are similar for all modes for a given value of s (emissions change by less than 17% for

any fixed value of s between cruise power and takeoff power, to be compared to around 50% change for ICAO emission indices), s must decrease as the power mode increases ($s_{CR} > s_{CO} > s_{TO}$). On the other hand, soot emissions increase with unmixedness. The typical trend for high powers is that soot increases with power so that s should follow the same trend. Therefore, we should get $s_{CR} < s_{CO} < s_{TO}$ to match soot ICAO emissions. This mismatch between unmixedness trends for soot and NO_x is too big in most of the cases so the model cannot predict accurately both soot and NO_x emissions at the same time. Indeed, optimizing emissions results for NO_x, CO and soot yields unmixedness values that make soot emission indices unstable as shown Figure 29.

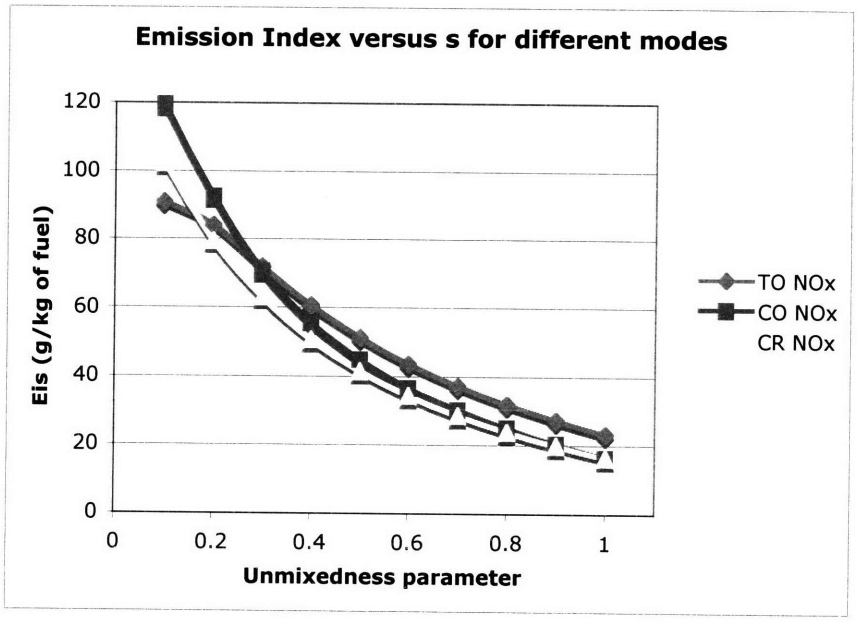


Figure 27 – Similarities of NOx emissions for different modes, relation between unmixedness and NOx EI

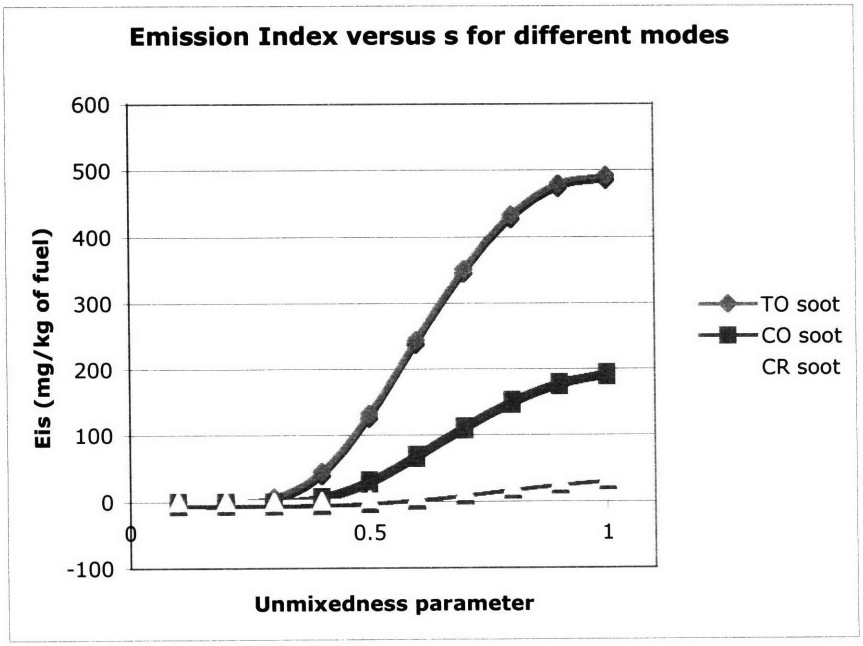


Figure 28 – Soot emission indices as function of unmixedness for different modes, relation between unmixedness and soot EI

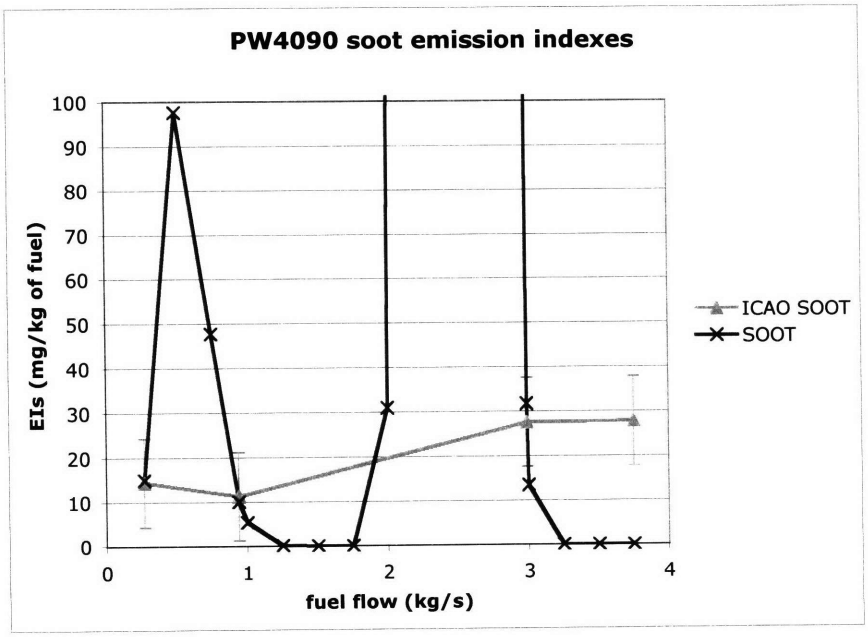


Figure 29 – Ultra sensitivity of the model when optimizing both soot and NO_x emissions

The objective function must be changed in order to model soot emissions. We must model independently NO_x and soot. First, we run an optimizing code using the previous

objective function for NO_x and CO only. This run sets the "internal" parameters. All "internal" parameters are kept the same for the soot model (volume and air fractions) except the unmixedness parameters. Unmixedness parameters are changed and obtained by minimizing the function $f_{soot} = \sum_{i=1}^{4} \left(\frac{Model_EIsoot_i - ICAO_EIsoot_i}{\sum_{i=1}^{4} ICAO_EIsoot_i} \right)^2$ with i representing the 4 ICAO LTO modes. This function also fixes the multiplicative coefficients that are applied to the mass and particle soot rates found in paragraph 3.3.6.

Improvements are seen when the soot model is optimized independently from the NO_x model (as described above) as shown in Figure 30 and Figure 31 (whiskers show ICAO data uncertainties). The soot model does not provide precise results when it is optimized for both NO_x and soot, but shows encouraging results when it is optimized independently. This process is used in the following.

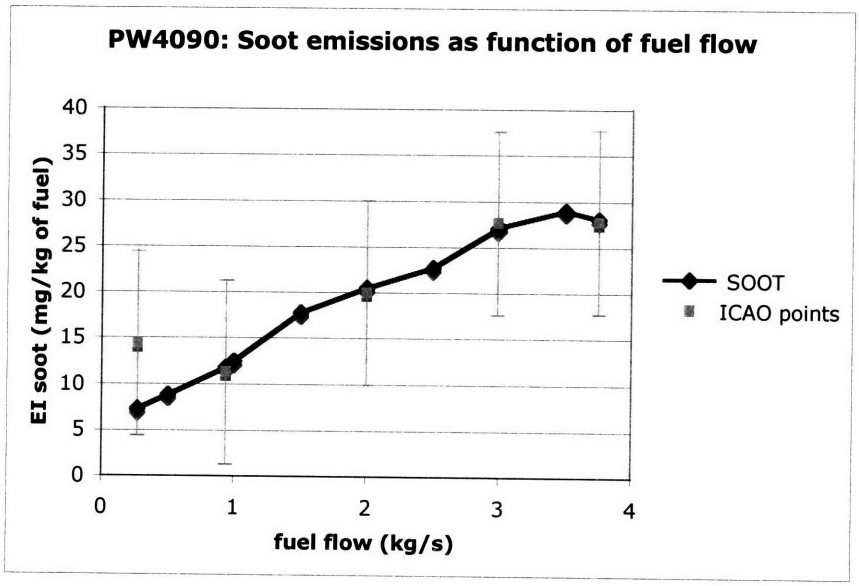


Figure 30 – PW4090: Soot emissions as function of fuel flow.

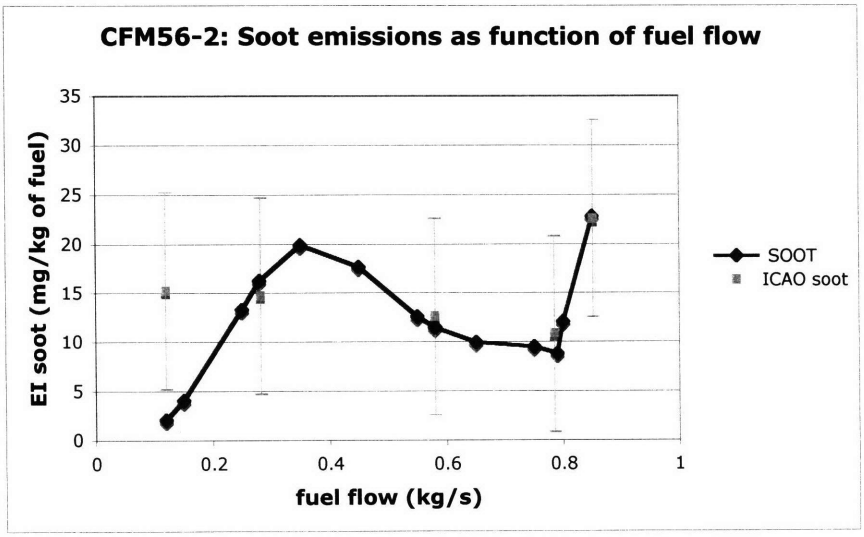


Figure 31 – CFM56-2C: Soot emissions as function of fuel flow. Note that low power problems are also found in the NO_x model.

5.3. Problems of Sensitivity to Input Variables

The combustor model can estimate soot emissions for a standard engine, but how sensitive is it relative to the input variables? The table below shows elasticity of different input parameters. Elasticity is defined as the percentage change of soot EI for a 1% change of the input parameter value.

Analyses show that the model is very sensitive to input data (Table 11) as values are relatively high. For instance, most of soot EIs change by more than 30% for a 1% change of the input value. This leads to uncertainties that are too high.

Variable	Elasticity
Temp.	-48.6
Pres.	-30.6
air mass flow	83.9
fuel mass flow	-34.6
volume	-48.4
Max eq. ratio	2.2
s	30.1
tau psr	13.4
tau plug	-23.8

Table 11 – Soot model elasticity of input variables for the PW4090 engine

When we combine uncertainties in input parameters – they are usually around 5% – with elasticities over 10 in absolute value, we obtain changes in soot EIs over 50% of the initial values. Because soot measurement uncertainties are around 30% of the initial value, elasticities over 10 are deemed to be too high for the input variable to yield results within the uncertainty limits. Therefore, we consider elasticities over 10 to be too high. On the contrary, we consider that the model is insensitive to an input variable when the elasticity of the variable is less than 1 in absolute value, as the resulting EI change is less than the input change.

The high elasticity values encountered in Table 11 are a consequence of soot oxidation. Indeed, the chemical species used by the soot model are insensitive to small input changes, and in the first phase, i.e. the primary zone where soot is formed, soot formation is relatively insensitive to input changes (elasticities are within the range [-5;5] for soot creation as shown in Figure 32).

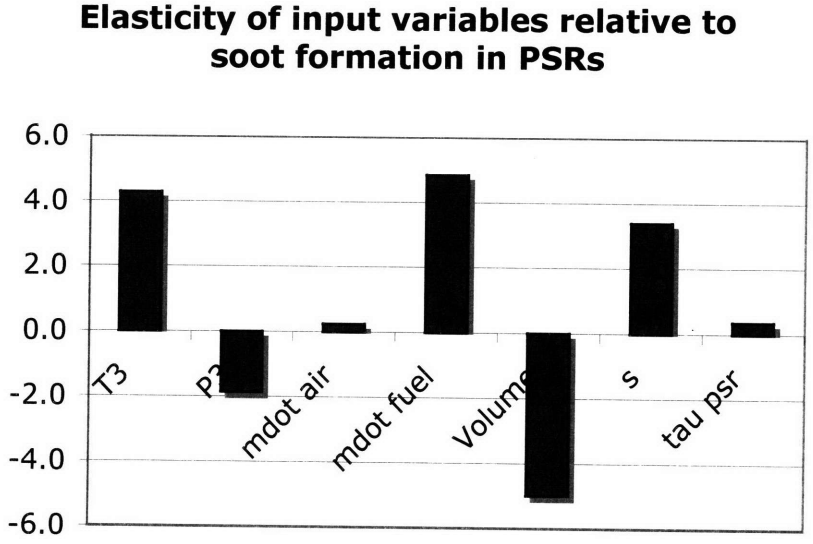


Figure 32 – Elasticity of input parameters relative to soot formation in PSRs

However, the oxidation part, especially the intermediate zone (plug #1), is very sensitive to any parameter change since elasticities are above 20. Elasticities of the variables inside the intermediate zone – i.e. temperature, soot flows inputs to Plug #1… –

can be as high as 80. Those levels of elasticities are obtained because the intermediate values of mass soot obtained after the primary zone are extremely high. For instance, emission index for the PW4090 combustor exhaust at takeoff is around 31,000 after the primary zone, whereas it is 27 in the exhaust. Therefore, a small change of the inputs in the intermediate zone, can have a large impact on the final soot EI value. After the intermediate zone, values of the soot EI lower to less than 900, so the sensitivity to the parameters is reduced. To sum up, because soot intermediate values are so high (see the unrealistic magnitude of the soot flow peak in Figure 33), the model yields the high elasticities encountered Table 11. Soot evolution as modeled is unrealistic as soot reaches a magnitude of about 0.1 kilogram per second inside the combustor.

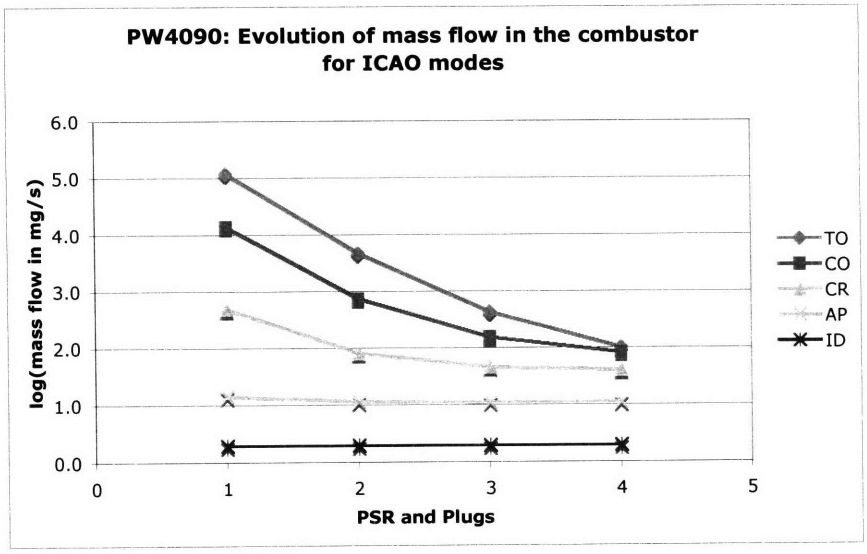


Figure 33 – Evolution of soot mass flow inside the PW4090 combustor model. Note the height of the peak.

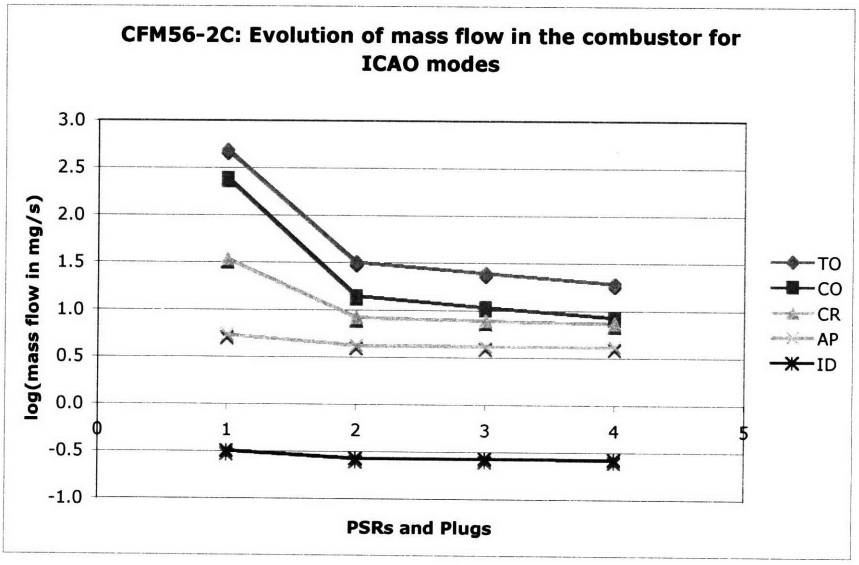


Figure 34 – Evolution of soot mass flow inside the CFM56-2C combustor model.

5.3.1. Sensitivity Correction and New Results

In order to lower the model sensitivity, i.e. the soot mass flow peak, we lower the soot growth coefficient and change the other coefficients. Intermediate soot mass flow is kept to a realistic maximum of 2 grams per second. The peak's height seems realistic as it is around 10 times larger than the exhaust value at takeoff, and less than 5 times larger for other modes as shown Figure 35. But we must mention this peak value is obtained by artificially lowering soot coefficients – both growth and oxidation – by as much as 100 times below the coefficients found in the literature as shown Table 12. The coefficients are issued from a combined optimization for the PW4090 and the CFM56-2C engine models. The objective function is the sum of the soot objective function found page 85 for the PW4090 and the CFM56-2C engines. Those coefficients are the same for both engines. Increasing stability of the inputs variables is made at the expense of similarities with the laminar models.

Soot Rate	**Multiplicative coefficient**
Soot nucleation (mass and particle rates)	3.16e-02
Soot growth	0.01
Soot oxidation	10

Soot coagulation	10

Table 12 – Multiplicative coefficients applied to the mass and particle soot rates found in paragraph 3.3.6

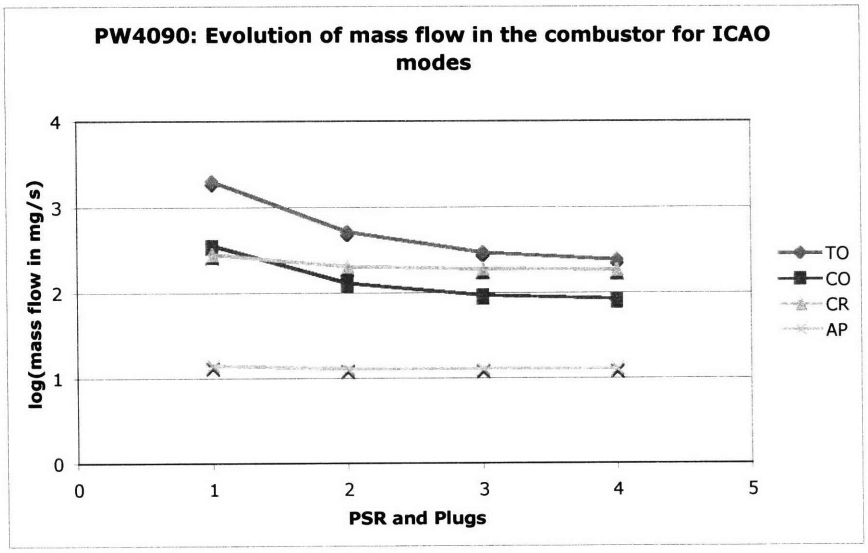


Figure 35 – Evolution of soot mass flow inside the new PW4090 combustor model

Figure 36 shows elasticity improvement for all parameters: the model is much less sensitive than the previous one. Input parameters elasticities are nevertheless on the edge of what we expect for the model. They are in the range [1;12] so output uncertainties can be as high as 60% (for an elasticity of 12 and an uncertainty of 5% for the input). As seen paragraph 1.4, uncertainties in soot emissions measurements are around 30%. The model emission uncertainty, although it is of the same order of the measurement uncertainties, is a bit too high.

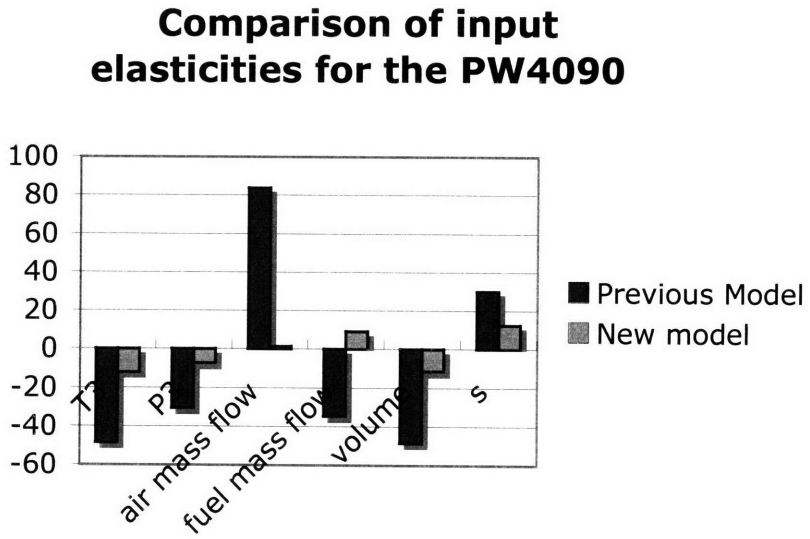


Figure 36 – Improvement of the model sensitivity for the PW4090 engine. The maximum absolute elasticity is 12.6 for the new model, compared to 83.9 for the previous one

New emissions for both engines are plotted Figure 37 and Figure 38. We note that the new model does not show the same similarity with ICAO data as found previously. This happens because emissions are less sensitive to unmixedness. Previously, emissions were so sensitive to this parameter that it was always possible to find a value that would generate the right amount of soot emission. This is not the case anymore.

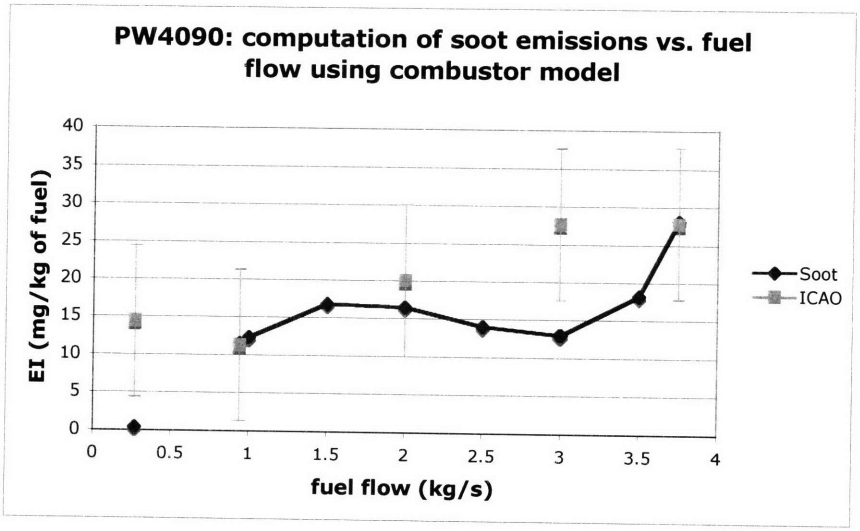


Figure 37 – PW4090: emission index evolution as function of fuel flow

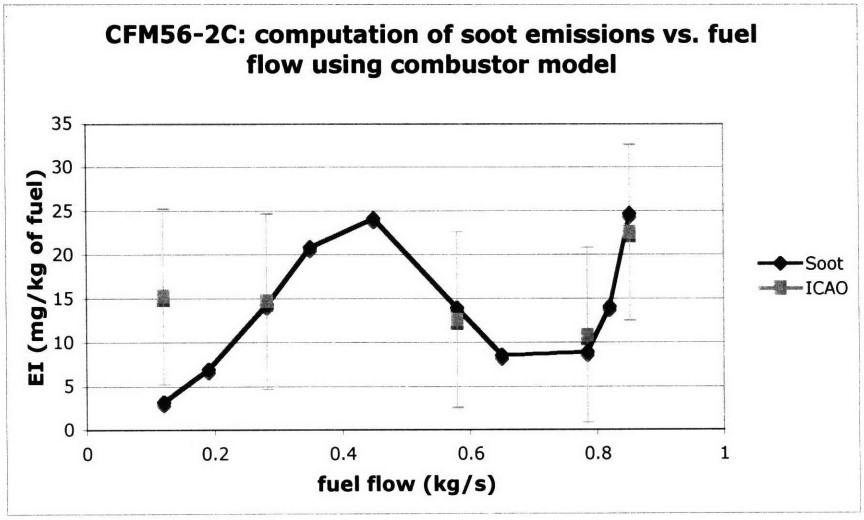


Figure 38 – CFM56-2C: emission index evolution as function of fuel flow

5.3.2. Interpretation and Precision Estimation of the Model

The "internal" parameters picked up by the optimizer are shown in Figure 39, Figure 40 and Figure 41. Results are generally consistent with intuition. First, in both engines, fractions of air and volume are similar in every zone (see height of blue and orange bars in Figure 39 and Figure 40). The main difference comes from the primary zone and intermediate zones fractions that are reversed for those engines. It models a smaller reaction zone for the CFM56-2C engine with earlier introduction of dilution and cooling air compared to the PW4090. The cooling zone properties – i.e. the dilution and the remaining zones – are similar for both engines. Further, Figure 41 shows unmixedness similarities for both engines. To sum up, these engine models show similarities relative to the "internal" parameters.

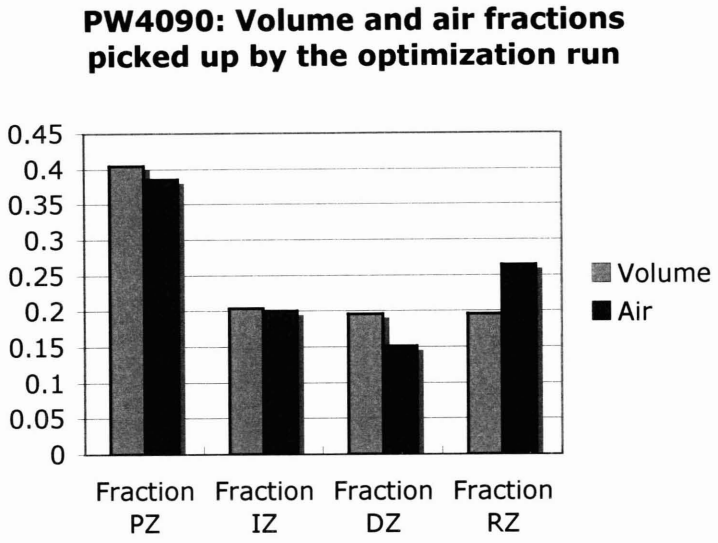


Figure 39 – PW4090: parameters picked by the optimizer for volume and air fractions

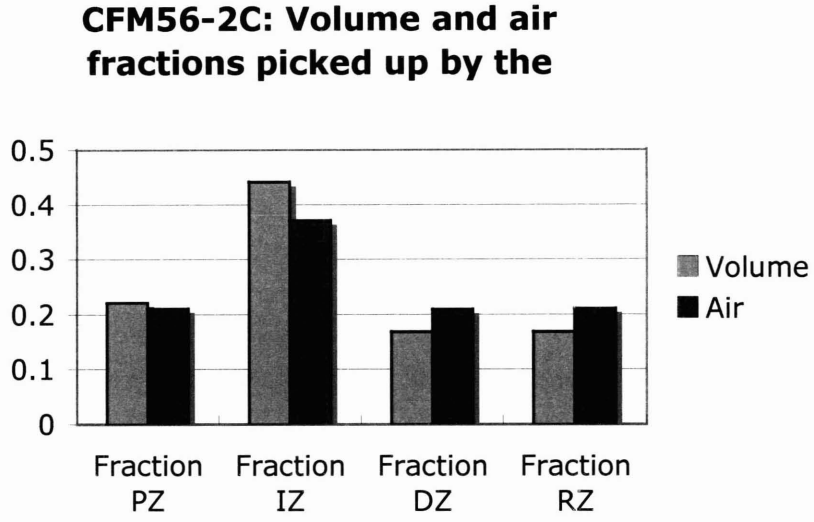


Figure 40 – CFM56-2C: parameters picked by the optimizer for volume and air fractions

Both modeled engines have different emission index trends. Emission indices of the CFM56-2C engine decrease with power and then increase for take-off, whereas emission indexes of the PW4090 engine increase with power, except for idle. This difference is not easy to capture for the model and yields different modeling precision as we can see seen Figure 37 and Figure 38. The CFM56-2C engine model is more precise than the PW4090 engine model. We can add that once the "internal" parameters are fixed with

the NO_x and CO objective function, the soot objective function yields a unique unmixedness value. Indeed, because soot emission indices grow as unmixedness parameters grow (see Figure 28), the minimum is unique.

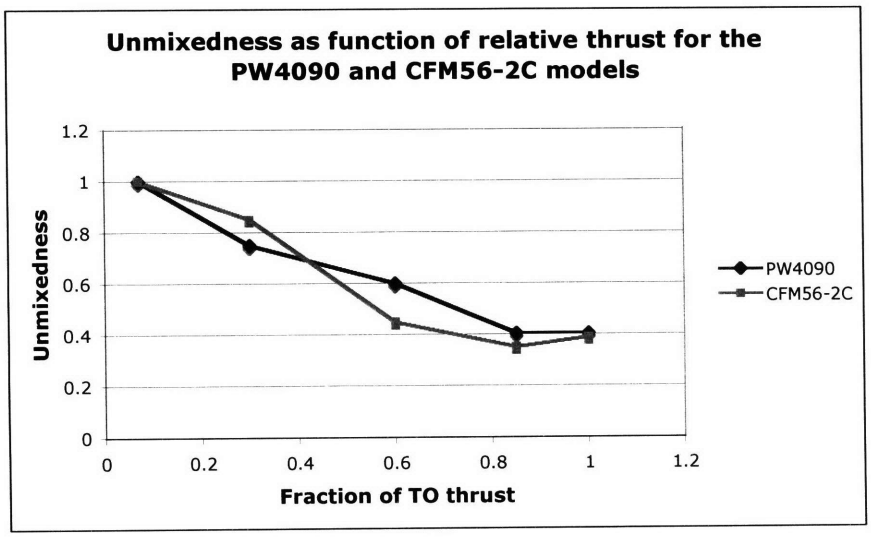


Figure 41 - Unmixedness as function of relative thrust for both engine models

Inside the combustor model, the general trend is that soot emissions increase until intermediate powers are reached – around cruise or mid fuel flow – and then emissions decrease until climb-out powers. Emissions for higher powers depend on unmixedness.

For low powers, oxidation is low and soot emissions increase due to a rise in temperature. It indeed makes acetylene and hydrogen emissions increase. Within this region, the model makes unmixedness decrease to avoid too much soot growth. In the second area, oxidation becomes important and counterbalances soot formation. Soot *EI* decreases with power.

For high powers, both soot growth and soot oxidation are established. Changing unmixedness does a modification of soot emission. If unmixedness increases, soot emission indexes increase and if unmixedness decreases, soot emission indexes decrease.

To sum up, soot emissions have similar shapes until climb-out as shown Figure 37 and Figure 38. For those two engines, soot increases in the first half, decreases and level off until climb-out and then evolves differently depending on the engine. Therefore, soot

modeling is more accurate when emissions follow the same trend as the model (just as the CFM56-2C engine).

This study requires analysis of more engine data to check the validity of the model and to confirm or not the shape of the function unmixedness vs. fraction of takeoff thrust. The final objective is to find a trend for this function that would be used to assess emissions of future engines and this cannot be done without more data. There is also the need to get more data on evolution of soot inside the combustor to tune the model coefficients with better accuracy.

Conclusion

Implementation of a soot mechanism in a simplified combustor model shows promising results as the optimized soot emission model, based on "internal" parameters from the NO_x model, approximate ICAO data for both the PW4090 and the CFM56-2C engines with limited uncertainties. The chosen model uses the HACA mechanism for soot growth, uses both OH and O_2 oxidation, and is based on the GRI Mech mechanism. Similarities between both engine emissions, between both unmixedness functions and between "internal" parameters are promising. For unmixedness, functions display a convex parabolic-like shape with values that are relatively close for both engines. For soot emissions, both models feature similar trends with emission indexes that increase, decrease and increase again with fuel flow. Emissions are consistent for both engines. However, this emission trend is consistent with the CFM56-2C – it achieves therefore good precision for this engine – but not with the PW4090. This a shortfall of the model.

Model emissions uncertainties are about the same as the measurement ones. They are large, (around 50%) and make soot emissions obtained with the model to be within the uncertainty range of the measurements. The question of whether this uncertainty is too large is a good question as high uncertainty gives low confidence in the changes obtained by the combustor model. More engine modeling is required to assess the capacity of the model to estimate diverse engine emissions.

We also need more information about the evolution of soot inside aircraft gas turbine engines. Obtaining the maximum soot mass flow for each power would allow us to set up soot coefficients with more accuracy and to check whether the model predicts the peak's height with precision. If the peak is lower than the one modeled, less sensitivity to the input variables can be achieved. This sensitivity issue is important because input data are obtained with a precision of 3% to 5%. As a consequence, relatively low elasticity – in the range [-6 ; 6] – is required for all parameters to stay within the 30% measurement uncertainties. The actual model uncertainties are slightly too high.

Appendixes

Appendix A: FOA Method 3.0 (from Roger L. Wayson, Gregg G. Fleming, Brian Kim and Julie Draper[9])

The FOA 3.0 breakdown by component led to a new general form of:

PMvols = F(Fuel Sulfur Content) + F(Fuel Organics) + F(Lubrication Oil)

PMnvols = SN v. Mass Relationship

TOTAL PM = PMvols + PMnvols

INDIVIDUAL COMPONENTS

Non-volatiles (soot)

The FOA 3.0 assumptions made were:

- As proven by multiple researchers, SN correlates to non-volatile PM mass emissions.[2]
- Average air-to-fuel ratios (AFR) per power setting[45] can be assumed for all commercial turbine jet aircraft as shown in Table 1 using input from manufacturers.
- Error in SN measurement by different researchers could be as great as ± 3 in extreme conditions. The actual measurements of the pollutants with different analyzers also have errors. However, a review of the standard deviations of the

[45] Eyers, C., CAEP/WG3/AEMTG/WP5, Improving the First Order Approximation (FOA) for Characterizing Particulate Matter Emissions from Aircraft Engines, Alternative Emissions Methodology Task Group (AEMTG) Meeting, Rio De Janeiro, Brazil.

measurement error reported for APEX1 show that the values are far less than the SN possible error. As such, allowing the SN to change by a value of ± 3 form upper and lower bounds to the estimate.

- A difference in the trends for SN and mass occur for those SNs ≤ 30 and those > 30. Most modern engines have SNs < 30 but older engines remain in the fleet and some method is necessary to allow prediction of these engines. As such, there must be a correlation for SN to mass for each of the four ICAO engine certification power settings as well as below and above a SN of 30, resulting in the use of eight equations.

The methodology is based on the available mass data at this time and is related to the smoke number (SN) so that emissions from the majority of jet turbine engines for commercial aircraft in the fleet can be approximated by using the ICAO emissions databank.

For the estimation of mass emissions for SNs less than 30, a correlation was used for measurement data developed by Dr. Hurley at Qinetiq in the United Kingdom. In-situ data from testing from DLR and the University of Missouri, Rolla were used for verification.

Table 1. Assumed Average Air-to-Fuel Ratios by Power Setting

Power Setting	AFR
7% (idle)	106
30% (approach)	83
85% (climbout)	51
100% (takeoff)	45

The analysis of these data, based on mass per volume of exhaust, yielded an equation to predict the concentration index (CI) as compared to the SN as follows:

$$CI = 0.0694(SN)^{1.23357} \quad [4]$$

Where: CI = concentration index (mg/M^3)
SN = smoke number ≤ 30

For SNs > 30 a different approach was utilized. In this case data from DLR in Germany as well as Hurley were used in the analysis.

$$CI = 0.0297(SN)^2 - 1.802(SN) + 31.94 \quad [5]$$

Where: SN = smoke number > 30

Final calculation of the non-volatile estimation of PM is based on two other derivations. The first is the calculation of the exhaust volume based on the AFR. This term is needed as a multiplier times the concentration index to allow an emission index directly tied to

fuel usage as is customary. While details are presented in the working paper by Eyers[46], the reduced equation is:

$$Q = 0.776(AFR) + 0.733 \qquad [6]$$

Where: Q = core exhaust volume (M^3)
AFR = modal air-to-fuel mass ratio

If the SN is measured with bypass air, the bypass ratio, _, will be used as a multiplier to estimate the exhaust volume. This would result in the form:

$$Q = \left[0.776(AFR) + 0.733\right](1 + \beta) \qquad [7]$$

From this, the non-volatile PM EI for non-volatiles may be calculated from:

$$EI_{non\text{-}vol} = Q\ (CI) \qquad [8]$$

Where: $EI_{non\text{-}vol}$ = emission Index (mg/kg fuel)
CI = emission concentration index (mg/M^3)

It is of note that upper limits were evaluated to provide a maximum bound to the predicted non-volatile EI and not necessarily as useable values. This was done by increasing the SN by a value of 3.

The equations that allow these conservative values are:

---

[46] Eyers, C., CAEP/WG3/AEMTG/WP5, Improving the First Order Approximation (FOA) for Characterizing Particulate Matter Emissions from Aircraft Engines, Alternative Emissions Methodology Task Group (AEMTG) Meeting, Rio De Janeiro, Brazil.

$$CI = 0.012(SN)^2 + 0.1312(SN) + 0.2255 \quad [9]$$

Where: SN = smoke number ≤ 30

$$CI = 0.0297(SN)^2 - 1.6238(SN) + 26.801 \quad [10]$$

Where: SN = smoke number > 30

One other problem exists. The ICAO database does not always contain complete SN information. A procedure was used based on dividing aircraft into groups by combustor design and using the trends of each group to fill in needed SNs.[47] Use of this method allows modal calculations and prediction of the non-volatile EIs for the four defined modes for most engines listed in the ICAO database. The term most is used since some reported SNs are zero which result in extremely low EI values.

EPAct MODIFICATIONS FOR NON-VOLATILE COMPONENT

> *Two conservative approaches were reviewed: (1) the use of certification smoke numbers presented in the ICAO data bank plus 3 smoke numbers to bound the upper limit that could occur in smoke number measurement (Equation 9 and 10) or (2) adding a factor for bypass flow using the best estimate approach (Equation 7). Approach 1 was eliminated because the addition of 3 to a certification smoke number was meant to form an upper bound and not based on real conditions. For the purposes of the EPAct Study, it was agreed to multiply the flow rate by the bypass ratio. This approach results in increased values that seem to agree the best with newer data such as from the Aircraft Particle Emission eXperiment (APEX) and it is more closely related to corrections used by manufacturers during certification where bypass flow may be included. It should be noted that this method assumes the non-volatile particulate matter is constant in the entire*

---

[47] W John Calvert, W.J., Revisions to Smoke Number Data in Emissions Databank, QinetiQ, Gas Turbine Technologies, 23 February 2006.

flow (core exhaust flow and bypass flow) and increases the value by as much as 8.59 using the ICAO bypass ratios.

Sulfur Component

The FOA3 assumptions made were:

- Sulfur emissions are primarily a function of fuel sulfur since no other major source of sulfur exits.
- Most sulfur results in gaseous emissions of SO_2 but some is converted from fuel sulfur to sulfuric acid (H_2SO_4). The total conversion requires a certain amount of residence time in the atmosphere and the sulfuric acid is being depleted at the same time by other atmospheric components. Sulfates would dominant PM found on an ambient air monitoring filter and a molecular weight of 96 for SO_4 was assumed.
- Sulfur contents of fuels change from location to location and should remain a variable during the estimation process. Default values can be defined, however, based on published values.[48]
- Conversion efficiencies also change from location to location but can be estimated and default values can be defined.[49]

These assumptions resulted in the form shown by Equation 11:

$$EI_{PMvols-FSC} = 1x10^6\left[\frac{FSC(\varepsilon)MW_{out}}{MW_S}\right] \quad [11]$$

Where: $EI_{PMvols\ -\ FSC}$ = EI for volatile fraction due to sulfur compounds emitted (mg/kg of fuel)

FSC = fuel sulfur content (% by weight)

[48] Coordinating Research Council, Inc., Handbook of Aviation Fuel Properties, Third Edition, CRC Report No. 635, Alpharetta, GA., 2004.

[49] Schumann, U., F. Arnolod, R. Busen, J. Curtius, B. Karcher, A. Kiendler, A. Petzold, H. Schroder, and K.H. Wohlfrom (2002). Influence of fuels sulfur on the composition of aircraft exhaust plumes: The experiments SULFUR 1-7, Jour. of Geophysical Research, 107:D15, 4247.

$_$ = S^{IV} to S^{VI} conversion rate as a fraction

MW_{out} = 96 for sulfates in exhaust

MW_S = 32 for sulfur

EPAct MODIFICATIONS FOR SULFATES:

The EPAct discussions were based on three topics: fuel sulfur content, conversion efficiency, and final product. The typical value for fuel sulfur content listed in the Handbook of Aviation Fuel Properties was selected which is 0.068%$_{mass}$ (680 ppmm). Conversion of gaseous sulfur species, primarily SO_2, occur creating particulate matter. While much more is involved, the gas-to-particle conversion process can be simply described by the following major chemical reactions:

$$SO_2 + O(+M) \rightarrow SO_3(+M)$$
$$SO_3 + O \rightarrow SO_2 + O_2$$
$$SO_2 + OH \rightarrow SO_3 + H$$
$$SO_2 + OH(+M) \rightarrow HOSO_2(+M)$$
$$HOSO_2 + O_2 \rightarrow SO_3 + HO_2$$
$$SO_3 + H_2O \rightarrow H_2SO_4$$

Of note is that sulfuric acid (H_2SO_4) is hydroscopic and will combine readily with atmospheric moisture resulting in a hydrated compound. Aircraft engine literature indicates that as low as one molecule of water per two of sulfuric acid or as much as two molecules of water per molecule of sulfuric acid could occur resulting in a heavier compound.[50,51] *Assuming a simple conversion efficiency for*

---

[50] Dakhel, P.M., S.P. Lukachko, I.A. Waitz, , R.C. Miake-Lye, and R.C. Brown (2005). Post-Combustion Evolution Of Soot Properties In An Aircraft Engine, Proc. Of GT2005, ASME Turbo Expo 2005: Power for Land, Sea and Air, Reno-Tahoe, NV., June 6-9.

[51] Arnold, F., T.H. Stilp, R. Busen, and U. Schumann (1998). Jet engine exhaust chemiion measurements implications for gaseous SO_3 and H_2SO_4, Atmospheric Environment, 32:18, 3073-3077.

this complex set of reactions, several literature references were reviewed and an upper limit value of 5% was selected[52,53]*. After discussion with the CMAQ modelling team, it was decided that the final product should not include hydration of H_2SO_4 since this is done as part of the CMAQ simulation process and that a molecular weight of 98 should be used as a modification of the term MW_{out} in Equation 11.*

Fuel Organic Emissions

The FOA3 assumptions made for PM fuel organics were:

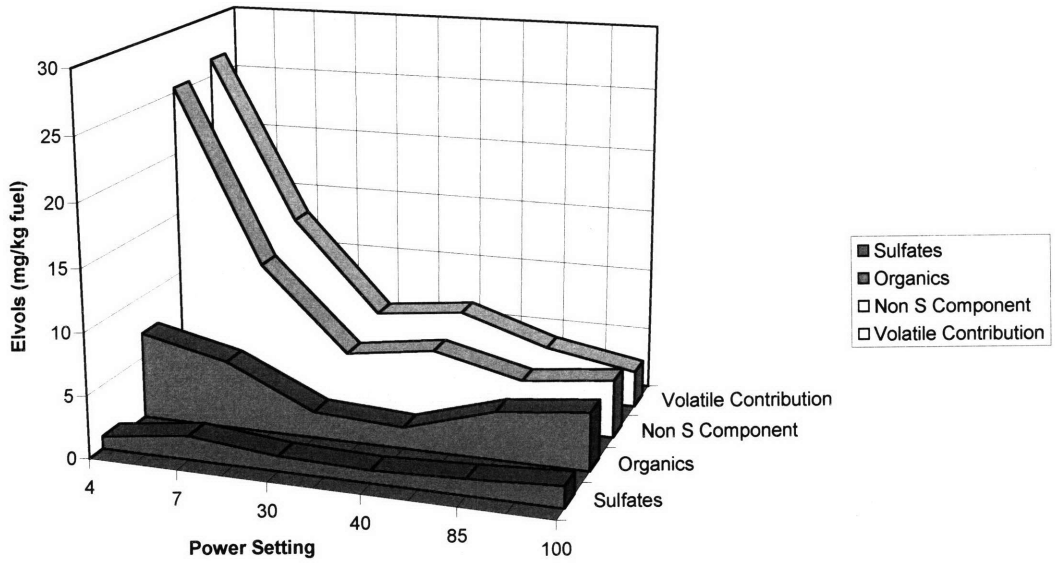
- Gas phase total hydrocarbons (HC) EIs are directly related to PM fuel organic emissions. That is, if unburned HC emissions increase, so do the overall PM organic emissions in a related fashion.
- Fuel PM organic emissions can be formed as a coating on non-volatile PM or due to condensation from the gas phase. This process is not well understood at this time and although these emissions are included, there is no separate calculation process.
- Measurement data separating the organic fraction from the overall PM emissions from in-service engines are very limited. Information from APEX1 would seem to be the most reliable at this time. However, only one engine (CFM56-2-C1) is included and it is assumed that the trends shown in Figure 1 are consistent for all commercial jet turbine engines in the ICAO database. As such, ICAO certification EIs for hydrocarbons can be related to the PM fuel organic emissions.
- The data used is for a probe 30 meters behind the aircraft. It is assumed that in this distance volatile organic PM emissions are representative of those in the atmospheric in the vicinity of airports since other data is not available.
- The overall estimation problem is multi-faceted & many details are not well known. As such, the organics methodology for PM fuel organics must be simplistic at this time.

---

[52] Sorokin, A., E. Katragkou, F. Arnold, R. Busen, and U. Schumann (2004). Gaseous SO_3 and H_2SO_4 in the exhaust of an aircraft gas turbine engine: measurements by CIMS and implications for fuel sulphur conversion to sulfur (VI) and conversion of SO_3 to H_2SO_4, Atmospheric Environment, 38, 449-456.

[53] Schumann, U., F. Arnold, R. Busen, J. Curtius, B. Karcher, A. Kiendler, A. Petzold, H. Schlager, F. Schroder, and K.H. Wohlfrom (2002). Influence of fuel sulfur on the composition of aircraft exhaust plumes: The experiments of SULFUR 1-7, Jour. of Geophysical Research, 107:D15, 4247.

Figure 1. Trends from APEX 1 for CFM56-2-C1 engine



The resulting "non S component" was derived by subtracting the "sulfates" from the "volatile contribution" except for the power settings of 85 and 100%. At these power settings, the values dropped below that shown as "organics" measured by a different instrument. In an attempt to not under-predict, the values of the "organics" curve shown in Figure 1 for 85 and 100% power settings were used directly. This resulted in Equation 12 with all modes defined for the "non S component."

$$PMvol_{fuel_organic} = \frac{Non_S_Component}{EI_{HC(CFM56-2C5)}}(EI_{HC(Engine)})$$

[12]

Where:

$PMvol_{fuel\ organic}$ = volatile PM emissions of organics (mg/kg fuel)

Non_S_Component = a constant ratio based on the trends shown in Figure 1.

$EI_{HC(CFM56)}$ = ICAO emission index for hydrocarbons for the CFM56 engine

$EI_{HC(Engine)}$ = specific ICAO emission index for hydrocarbons for the engine of concern

EPAct MODIFICATIONS ON FUEL ORGANICS:

The CFM56 scaling method was reviewed and it was decided that a true mass balance represented a more consistent approach across the entire power spectrum. It was also agreed that a margin of conservatism should be added to the resulting values from the mass balance approach. This required modifications in two steps.

Step 1: The measured volatile component derived from APEX1 data was used and adjusted for the sulfur component (shown as "sulfates" in Figure 1). In this approach, a single set of measurements was used to avoid conflicting data from different measurement techniques. This resulted in the curve shown as the "non S component" no longer being adjusted for the 85 and 100% power setting as was done in the FOA 3.0 approach described previously. Instead, the resulting curve used is simply the curve listed as the "volatile contribution" in Figure 1 is subtracted off the values of the "sulfates" at each engine power setting so that sulfur is not counted twice. Also, to be conservative, it is assumed that 100% of the resulting "volatile component" curve are semi-volatile and in the particle phase.

Step 2: To insure an even more conservative method, the APEX1 data set was further analyzed to determine total volatile PM. Again using the APEX1 data for the base fuel condition, the ratio of sulfur to organics was determined from reported measurements and this ratio used to subtract out the sulfate contribution from the total volatile PM. This resulted in a volatile PM component that did not include sulfur. These results are reported in Table 2.

Table 2. Derived "Non_S_Component values by mode [mg/ kg fuel]

Mode	***Volatile Contribution***	***Sulfates***	***Derived Non_S_Component***
Idle	*13.2*	*1.9*	*11.3*
Approach	*5.7*	*1.2*	*4.5*
Climbout	*4.2*	*1.3*	*2.9*
Takeoff	*2.9*	*1.7*	*1.2*

The standard deviation of the individual data points for this derived volatile component, without sulfates, was then computed (see Table 3) and added to the new derived "non S component". This new, more conservative, "non-S component" was used in Equation 12 to calculate the EI for PM organics.

This is shown in equation form as:

$$(Total\ PM - Non\text{-}volatile\ PM)(1-(sulfate/organics)) = PM_{non\text{-}S\ organics}$$

$$Standard\ deviation(PM_{non\text{-}S\ vol}) + non\ S\ component\ (Figure\ 1) = Modified\ non\ S\ component\ (to\ be\ used\ in\ Equation\ 12)$$

Table 3. Computed standard deviations for the volatile PM component

Mode	***Std. Dev. [mg/ kg fuel]***
Idle	*25*
Approach	*10*
Climbout	*16*
Takeoff	*19*

Lubrication Oil

Emissions of lubrication oil are not well documented in the literature. As such, an approximation method for this component was not included in the FOA 3.0.

EPAct DECISION ON LUBRICATION OIL:

Data was extremely scarce and multiple engineering judgements had to be made based on data supplied by an engine manufacturer. Lubrication oil use increases with engine wear until a critical value of about 0.3 quarts per hour occurs. At this time, the engine is removed from service for substantial reworking and maintenance. Based on an assumption that about 0.1 of the value used for overhaul standards represents nominal operating consumption, it was determined that approximately 0.03 quarts per hour of lubrication oil are lost. Since venting is the primary release and tends to occur at the higher power settings, a ratio of the time in takeoff (0.7 minutes) and climb-out (2.2 minutes) modes were used and it was found that 0.00145 quarts could be emitted during these operations in the vicinity of airports. Using a specific gravity of 1.0035 reported for Mobil Jet Oil II (density = 1,003.5 kg/m^3 or 949.7 grams/quart)[54], it was found that approximately 1.4 grams of lubrication oil volatile organic PM could be released per landing and takeoff operation (LTO). This value is added to the volatile PM contribution from fuel organics to determine the total organic volatile component for input into the CMAQ model. Sulfur volatile emissions are handled separately in the EPAct method and this is also required by the CMAQ model.

The estimation of the lubrication oil emissions in equation form is:

*Nominal consumption = 0.3 quarts/hr * 0.1 = 0.03 quarts/hr*

*Emissions per LTO = 0.03 quarts/hr * 1 hour/60 min * 2.9 min/LTO*
= 0.00145 quarts/LTO

*Emissions (grams/LTO) = 0.00145 quarts/LTO * 949.7 grams/quart*

≈ 1.4 grams of volatile PM from lubrication oil per LTO

---

[54] 1,003.5 kg/m^3 * 1 m^3/1,056.7 quarts * 1,000 grams/1 kg = 949.7 grams/quart

Appendix B: Chemical Species used in GRI-Mech[43]

(Chemical Formula + Molecular Weight)

H2 2.01588	CH2OH 31.034	NO2 46.010
H 1.00794	CH3O 31.034	N2O 44.020
O 15.9994	CH3OH 32.042	HNO 31.018
O2 32.000	C2H 25.028	CN 26.020
OH 17.00734	C2H2 26.03728	HCN 27.028
H2O 18.01528	C2H3 27.044	H2CN 28.036
HO2 33.008	C2H4 28.052	HCNN 41.038
H2O2 34.016	C2H5 29.060	HCNO 43.028
C 12.01	C2H6 30.068	HOCN 43.028
CH 13.018	HCCO 41.028	HNCO 43.028
CH2 14.026	CH2CO 42.036	NCO 42.020
CH2_S 14.026	HCCOH 42.036	N2 28.013
CH3 15.034	N 14.010	AR 39.950
CH4 16.042	NH 15.018	C3H7 43.086
CO 28.0101	NH2 16.026	C3H8 44.094
CO2 44.0095	NH3 17.034	CH2CHO 43.044
HCO 29.018	NNH 29.028	CH3CHO 44.052
CH2O 30.026	NO 30.010	

Appendix C: Chemical Species used in GRI-Mech Jet-Fuel Mechanism[44]

(Chemical Formula)

H	C2H6	C4H5(I)	C5H4O	C5H10(1)
O2	C2H5	C4H6(S)	C5H6(L)	C5H11(1)
OH	C2HO	C4H6(T)	C5H5(L)	C6H13(1)
O	CH3O	C4H6O(A)	C5H4(L)	C6H13(2)
H2	CH3OH	C4H6(B)	C5H3(L)	C6H12(1)
H2O	C2H	C4H6O(B)	C5H2	C6H11
HO2	C2O	C6H4(L)	C2H3O	C7H16
H2O2	C4H4	C6H6(A)	C3H3O	C7H15(1)
CO2	C3H2O	C6H6(B)	C4H6(M)	C7H15(2)
CO	C3H4(A)	C6H6(S)	C4H6(F)	C7H15(3)
CH	C3H4(P)	C6H7(L)	C6H8	C7H15(4)
CHO	C3H5(A)	C6H5(B)	C3H5O	C7H14(1)
CH2OH	C3H5(S)	C6H6	C3H6O	C7H14(2)
CH2O	C3H5(T)	C6H3	C3H6OH	C7H14(3)
C2H2O	C3H4O	C6H4	C2H4O	C7H13
CH2(T)	C3H7(N)	C6H5(A)	C3H6O(A)	C8H16
C2H2	C3H8	C6H5	C3H6O(P)	C8H17(1)
CH3	C3H7(I)	C6H5O	C3H5O(A)	C8H17(2)
C2H3	C4H3(N)	C6H6(M)	C3H5O(P)	C8H17(3)
CH4	C4H3(I)	C6H6(F)	C3H5O(T)	C8H17(4)
C2H4	C4H2	C6H6(D)	C4H4O	C8H18
C3H	C6H2	C6H5OH	C5H	C2C2H9
C3H2	C8H2	C5H5	C	C2C2H8
CH2(S)	C4H	C5H6	C4H7	C4H10(N)
C3H3	C4H2O	C6H7	C4H8(1)	C4H10(I)
C3H4(B)	C4H5(S)	C5H5O	C4H9(P)	N2
C3H6	C4H5(T)	C5H4OH	C5H9	

NOx Mechanism

N
NH3
NH2
NH
NO
NO2
N2H2
NNH
N2O
HNO
HCN
CN
NCO
HNCO
HOCN
HNO2
NO3
H2CN
CH3NH2
CH3NO
CH2NOH
HNO3
HNC
HCNO
C7H8

Aromatic Mechanism

C6H5CO
C7H7
C7H6H
OC7H7
HOC7H7
C7H6O
C7H7OH
C8H8
C14H14
C8H10
C8H9
C8H6
C8H7
C7H7O
CC6H7
C7H6
C7H7OO
C8H5
CC7H5
CC7H7

Appendix D: Nagle and Strickland-Constable Oxidation Equation[35]

The equation models soot oxidation (w_{O_2}) as a function of O_2 pressure and temperature:

$$w_{O_2} = -\left(\left(\frac{k_A p_{O_2}}{1 + k_Z p_{O_2}}\right)\chi + k_B p_{O_2}(1-\chi)\right)$$

where p_{O_2} is the oxygen pressure in atmospheres, $\chi = \frac{1}{1 + k_T p_{O_2} / k_B}$,

$k_A = 2 \cdot 10^4 e^{-130{,}000/RT}$, $k_B = 4.46 e^{-64{,}000/RT}$, $k_T = 1.51 \cdot 10^8 e^{-406{,}000/RT}$ and $k_Z = 2.14 \cdot 10^4 e^{17{,}000/RT}$.